การพัฒนาอุปกรณ์วิเคราะห์ไมโครฟลูอิดิกสำหรับการตรวจวัดสารประกอบซัลเฟอร์โดยใช้รามานสเปกโทรสโกปี

นางสาวดวงทิพย์ ลาวัณย์เสถียร

วิทยานิพนธ์นี้เป็นส่วนหนึ่งของการศึกษาตามหลักสูตรปริญญาวิทยาศาสตรดุษฎีบัณฑิต
สาขาวิชาเคมี ภาควิชาเคมี
คณะวิทยาศาสตร์ จุฬาลงกรณ์มหาวิทยาลัย
ปีการศึกษา 2560

DEVELOPMENT OF MICROFLUIDIC ANALYTICAL DEVICE FOR DETECTION OF SULFUR-CONTAINING COMPOUNDS USING RAMAN SPECTROSCOPY

Miss Duangtip Lawanstiend

A Dissertation Submitted in Partial Fulfillment of the Requirements
for the Degree of Doctor of Philosophy Program in Chemistry
Department of Chemistry
Faculty of Science
Chulalongkorn University
Academic Year 2017

Thesis Title	DEVELOPMENT OF MICROFLUIDIC ANALYTICAL DEVICE FOR DETECTION OF SULFUR-CONTAINING COMPOUNDS USING RAMAN SPECTROSCOPY
By	Miss Duangtip Lawanstiend
Field of Study	Chemistry
Thesis Advisor	Monpichar Srisa-Art, Ph.D.
Thesis Co-Advisor	Assistant Professor Kanet Wongravee, Ph.D.

Accepted by the Faculty of Science, Chulalongkorn University in Partial Fulfillment of the Requirements for the Doctoral Degree

.....Dean of the Faculty of Science

(Associate Professor Polkit Sangvanich, Ph.D.)

THESIS COMMITTEE

.....Chairman

(Associate Professor Vudhichai Parasuk, Ph.D.)

.....Thesis Advisor

(Monpichar Srisa-Art, Ph.D.)

.....Thesis Co-Advisor

(Assistant Professor Kanet Wongravee, Ph.D.)

.....Examiner

(Professor Orawon Chailapakul, Ph.D.)

.....Examiner

(Professor Sanong Ekgasit, Ph.D.)

.....External Examiner

(Assistant Professor Yupaporn Sameenoi, Ph.D.)

ดวงทิพย์ ลาวัณย์เสถียร : การพัฒนาอุปกรณ์วิเคราะห์ไมโครฟลูอิดิกสำหรับการตรวจวัดสารประกอบซัลเฟอร์โดยใช้รามานสเปกโทรสโกปี (DEVELOPMENT OF MICROFLUIDIC ANALYTICAL DEVICE FOR DETECTION OF SULFUR-CONTAINING COMPOUNDS USING RAMAN SPECTROSCOPY) อ. ที่ปรึกษาวิทยานิพนธ์หลัก: อ. ดร.มนพิชา ศรีสะอาด, อ.ที่ปรึกษาวิทยานิพนธ์ร่วม: ผศ. ดร.คเณศ วงษ์ระวี, 83 หน้า.

ในงานวิจัยนี้ระบบไมโครฟลูอิดิกส์ร่วมกับการตรวจวัดด้วยรามานสำหรับการประยุกต์ในงานด้านการวิเคราะห์ได้ถูกพัฒนาขึ้นโดยใช้อนุภาคไมโครซิลเวอร์นาโนพอรัสที่สังเคราะห์ทั้งนอกและในชิปสำหรับเป็น SERS ซับสเตรต อนุภาคไมโครซิลเวอร์นาโนพอรัสที่สังเคราะห์นอกชิป ถูกนำมาใช้เป็น SERS ซับสเตรตบนชิปสำหรับการตรวจวัดกลูธะไธโอน โดยใช้เทคนิคการรายงานผลแบบย้อนกลับ อนุภาคไมโครซิลเวอร์นาโนพอรัสจะถูกหยดลงบนช่องทางเดินสารรูปกากบาทของระบบไมโครฟลูอิดิกส์ โรดามีนหกจี (ตัวรายงาน) จะเกิดอันตรกิริยากับอนุภาคไมโครซิลเวอร์นาโนพอรัสที่ฝังอยู่ในช่องทางเดินสาร เกิดเป็นสารประกอบเชิงซ้อนของโรดามีนหกจี-อนุภาคไมโครซิลเวอร์นาโนพอรัส ซึ่งให้สัญญาณรามานสูง จากนั้นโรดามีนหกจีในสารประกอบเชิงซ้อนจะถูกแทนที่ด้วยโมเลกุลของกลูธะไธโอน ทำให้สัญญาณของรามานลดลง ซึ่งการลดลงของสัญญาณรามานจะสัมพันธ์กับปริมาณกลูธะไธโอนที่เพิ่มขึ้น ช่วงความเข้มข้นที่เป็นเส้นตรงของวิธีวิเคราะห์สำหรับการตรวจวัดกลูธะไธโอน อยู่ในช่วง 10^{-8} - 10^{-3} โมลาร์ และมีค่าสัมประสิทธิ์ความเป็นเส้นตรงเท่ากับ 0.9760 โดยความเข้มข้นของกลูธะไธโอนที่จุดต่ำสุดของกราฟมาตรฐานคือ 10^{-8} โมลาร์ อนุภาคไมโครซิลเวอร์นาโนพอรัสที่ฝังอยู่ในช่องทางเดินสารสามารถนำกลับมาใช้ซ้ำได้ถึงสามครั้งโดยการล้างด้วยโซเดียมโบโรไฮไดร์ นอกจากนี้อนุภาคไมโครซิลเวอร์นาโนพอรัสยังถูกสังเคราะห์บนชิป โดยใช้คลอไรด์เป็นตัวเหนี่ยวนำให้ตกตะกอนของสารประกอบเชิงซ้อนซิลเวอร์แอมมีนเพื่อให้เกิดแม่แบบซิลเวอร์คลอไรด์ และตามด้วยปฏิกิริยารีดักชัน การเปลี่ยนแปลงอัตราการไหลของตัวทำปฏิกิริยา (สารตั้งต้น) ในระบบจะสังเกตพบโครงสร้างของแม่แบบซิลเวอร์คลอไรด์ที่แตกต่างกัน 4 แบบ ได้แก่ ลูกบาศก์, พีระมิดฐานสามเหลี่ยม, สามขา และ สี่ขา จากนั้นแม่แบบซิลเวอร์คลอไรด์จะถูกรีดิวซ์เพื่อให้เกิดเป็นอนุภาคไมโครซิลเวอร์นาโนพอรัส พบว่าโซเดียมโบโรไฮไดรด์เป็นตัวรีดิวซ์ที่ดีที่สุดเพราะว่าสามารถคงรูปร่างเดิมของแม่แบบซิลเวอร์คลอไรด์ไว้ได้ ผลการทดลองจาก SEM แสดงขนาดของการเชื่อมต่อของอนุภาคระดับนาโนบนผื้นผิวอยู่ในช่วง 40-65 นาโนเมตร โครงสร้างแบบสี่ขาของอนุภาคไมโครซิลเวอร์นาโนพอรัสซึ่งให้สัญญาณรามานสูงสุดจะถูกเลือกมาใช้เป็น SERS ซับสเตรตสำหรับการตรวจวัดไธโอไซยาเนตบนชิป ช่วงความเป็นเส้นตรงของวิธีวิเคราะห์นี้สำหรับการตรวจวัดไธโอไซยาเนตอยู่ในช่วง 1-20 ไมโครโมลาร์ และสัมประสิทธิ์ความเป็นเส้นตรงคือ 0.9887 ขีดจำกัดการตรวจวัดและขีดจำกัดการวิเคราะห์เชิงปริมาณที่ได้จากการคำนวณได้คือ 0.10 และ 1.5 ไมโครโมลาร์ ตามลำดับ ความถูกต้องของการวิเคราะห์ถูกศึกษาโดยการหาร้อยละการได้กลับคืนของสารละลายมาตรฐานไธโอไซยาเนต พบว่าอยู่ในช่วง 90-110% นอกจากนี้เปอร์เซ็นต์ความเบี่ยงเบนมาตรฐานสัมพัทธ์ของสัญญาณรามานในการตรวจวัดโพแทเซียมไธโอไซยาเนตในตัวอย่างน้ำลายมีค่าน้อยกว่า 9% สำหรับการตรวจวัดภายในวันเดียวกันและระหว่างวัน ดังนั้นวิธีที่พัฒนาขึ้นโดยใช้เทคนิค SERS ควบคู่กับไมโครฟลูอิดิกส์สำหรับการตรวจวัดสารไธโอไซยาเนตพบว่ามีความแม่นและความเที่ยงสูง

ภาควิชา เคมี	ลายมือชื่อนิสิต .....
สาขาวิชา เคมี	ลายมือชื่อ อ.ที่ปรึกษาหลัก .....
ปีการศึกษา 2560	ลายมือชื่อ อ.ที่ปรึกษาร่วม .....

5472891423 : MAJOR CHEMISTRY
KEYWORDS: MICROFLUIDIC ANALYTICAL DEVICE

DUANGTIP LAWANSTIEND: DEVELOPMENT OF MICROFLUIDIC ANALYTICAL DEVICE FOR DETECTION OF SULFUR-CONTAINING COMPOUNDS USING RAMAN SPECTROSCOPY. ADVISOR: MONPICHAR SRISA-ART, Ph.D., CO-ADVISOR: ASST. PROF. KANET WONGRAVEE, Ph.D., 83 pp.

In this work, microfluidic systems coupled with Raman detection for analytical applications were developed using both off-chip and on-chip synthesized nanoporous Ag microstructures (np-AgMSs) as SERS substrates. Off-chip synthesized np-AgMSs were used as on-chip SERS substrates for determination of glutathione (GSH) using a reversed reporting technique. The np-AgMSs were drop casted onto the cross channel of a microfluidic device. R6G (a Raman reporter) interacted with the embedded np-AgMSs in the microchannel to form R6G-np-AgMSs which provided high SERS signal. Then, R6G in the R6G-np-AgMSs complex was replaced by GSH, causing the decrease in SERS signal which was related to the GSH concentration. A linear range of the method for determination of GSH was found to be 10^{-8}-10^{-3} M with R^2 = 0.9760 and the lowest of calibration curve was 10^{-8} M. The embedded np-AgMSs could be reused up to 3 cycles by chemical regeneration using $NaBH_4$. In addition, np-AgMSs were also on-chip synthesized using Cl^- induced precipitation of a silver ammine complex ($[Ag(NH_3)_2]^+$) to form AgCl templates and followed with chemical reduction. By simply changing input reactant flow rates, four different structures of fabricated AgCl templates, including cubic, tetrahedron, tripod and tetrapod, were observed. The obtained AgCl templates were subsequently chemically reduced to form np-AgMSs. $NaBH_4$ was found to be the best reducing agent to reduce AgCl templates because it retained the structure of the parent AgCl templates. SEM results showed that the interconnected grain size of np-AgMSs was in the range of 40-65 nm. Tetrapod np-AgMSs which provided the highest SERS signal were chosen as SERS substrates for on-chip quantitative determination of SCN^-. A linear range of this approach for determination of SCN^- was in the range of 1-20 μM with R^2 = 0.9887. Calculated LOD and LOQ were 0.10 and 1.5 μM, respectively. For accuracy study, %recovery of spiked SCN^- standard solutions was found to be in the range of 90-110%. In addition, %RSD of SERS signal for the detection of KSCN in saliva was less than 9% for both intraday and interday measurements. The developed SERS-microfluidic method for the determination of SCN^- was found to be high accuracy and precision.

Department:	Chemistry	Student's Signature	.....
Field of Study:	Chemistry	Advisor's Signature	.....
Academic Year:	2017	Co-Advisor's Signature	.....

ACKNOWLEDGEMENTS

Firstly, I would like to express my deepest appreciation to my advisor, Dr. Monpichar Srisa-Art, for everything she has been doing for me since day one. Her overwhelming kindness was guiding me to be a better person and also her love with unconditional to lab students was impressed me. Without her encouragement and beveling in me, I could not success. Moreover, special thanks to my co-advisor, Assistant Professor Dr. Kanet Wongravee for his encouragement and guidance.

Besides my advisors and co-advisor, I would like to thank all committee including Associate Professor Dr. Vudhichai Parasuk, Professor Dr. Orawan Chailapakul, Professor Dr. Sanong Ekgasit and Assistant Professor Dr. Yupaporn Sameenoi for giving me guidance.

I gratefully acknowledge the financial support from the Science Achievement Scholarship of Thailand (SAST), Optical Spectroscopy and Electrochemistry Center of Excellence (EOSCE) and Sensor Research Unit (SRU).

Finally, I would like to thank my beloved friend, all lab members and my family for support.

CONTENTS

Page

Page

Page

LIST OF TABLES

LIST OF FIGURES

LISTS OF ABBREVIATIONS

%recovery	Recovery percentage
%RSD	Percentage of relative standard deviation
^0C	Degree Celcius
AgNPs	Silver nanoparticles
$AgNO_3$	Silver nitrate
AOAC	Association of official agricultural chemists
$C_6H_8O_6$	Ascorbic acid
$Cu(OAC)_2$	Copper(II) acetate hydrate
CTAB	Cetyltrimethylammonium bromide
E^0	Reduction potential
EFs	Enhancement factor
EDS	Energy dispersive X-ray spectroscopy
GSH	Glutathione
μTAS	Miniaturized total analysis systems
KSCN	Potassium thiocyanate
K_f	Complex formation constant
LOD	Limit of detection
LOQ	Limit of quantitation
LSPR	Localized surface plasmon resonance
Milli-Q	Deionized water
$NaBH_4$	Sodium borohydride
NaCl	Sodium chloride

N_2H_2	Hydrazine
NH_4OH	Ammonium hydroxide
np-AgMSs	Nanoporous Ag microstructure
PATP	*p*-aminothiophenol
PDMS	Polydimethylsiloxane
POC	Point of care
PVC	Polyvinyl chloride
R^2	Correlation coefficient
R6G	Rhodamine 6 G
SEM	Scanning electron microscope
SERS	Surface enhanced Raman scattering
SEI	Secondary electron image
SCN^-	Thiocyanate

CHAPTER I
INTRODUCTION

1.1 Introduction

Microfluidic systems or miniaturized total analysis systems (μTAS) have been used as analytical tools for several fields of applications including chemistry, biology, environment and point-of care (POC) diagnostics [1-4]. The μTAS systems offer practical advantages over conventional bench top systems, such as high sensitivity, online detection, easy manipulation, possibly automated systems and high-throughput analysis [5, 6]. Besides analytical applications, microfluidic systems have been widely used as microreactors for synthesis of various compounds, such as organic molecules [7], polymers [8-10] and nanoparticles [11-13]. Microfluidics offers advantages over batch synthesis in terms of high repeatability [14], monodispersity of nanoparticles [15] and high-throughput systems [16]. Flow rate is one of the most important factors in microfluidic systems. Concentration of reactant can be manipulated only by changing the input flow rate. Moreover, a flow-based system provides possibility of an automatic system to reduce the use of human labor [1]. The key parameter for microfluidic synthesis is the volume involving in microfluidic systems, which is down to nanoliters. Therefore, mass and heat transfers in micronscales are massively improved when compared to batch systems [17]. For batch synthesis, to obtain high quality products, vigorously stirring of the solutions and well and precisely controlling of experimental parameters are needed.

In terms of using microfluidics as an analytical device, a detection system is one of the important factors to be considered. Due to small volumes in microfluidic devices, a highly sensitive detection system is required. Surface enhanced Raman scattering (SERS) is one of the highly sensitive detection methods, which provides an enhancement factor (EFs) of 10^6-10^{14} times of Raman signal compared to a normal Raman scan [16, 18]. Characteristic vibration modes for individual functional groups on an analyte compound can be obtained by the technique, which offers high selective detection. Only small amount of analyte (down to 1 μL) is required. Furthermore, the

Raman spectrum of water is weak and unobtrusive, allowing good spectra of analytes to be acquired in aqueous solutions. According to all advantages, the SERS technique is very compatible with microfluidic systems for both in- and on-line detection systems.

In this work, we not only focused on the use of microfluidics coupled with Raman detection as an analytical device, but also focused on the use of microfluidics as a microreactor to on-chip synthesized nanoparticles to be used as on-chip SERS substrates for analytical applications.

1.2 Literature Review

Examples of reports on integration of SERS and microfluidic systems are evaluation of mixing behavior between confluent laminar flows in a microflidic channel [6], in situ monitoring of chemical reactions in a microfluidic channel [5], pharmaceutical and environmental analysis [4], biological analysis and biomedical diagnostics [2, 3]. Recent works were focused on on-chip synthesis of nanoparticles to be used as on-chip SERS substrates for in-situ detection. For example, Oh and Jeong [19] reported the use of plasmonic nanoprobes self-aligned along with microfluidics for detection of dopamine. Silver film was coated onto the surface of a polydimethyl siloxane (PDMS) device and the device was then treated with plasma and bonded with a glass slide. Results showed that the role of plasma was for PDMS bonding and for improving the plasmon resonance property of the embedded silver thin film. An SEM image in **Fig. 1.1** shows that after oxygen plasma treatment, an ordinary silver thin film was turned into nanotips and nanodots. Therefore, sensitivity of SERS signal was improved. This system could detect dopamine down to the concentration of 100 μM.

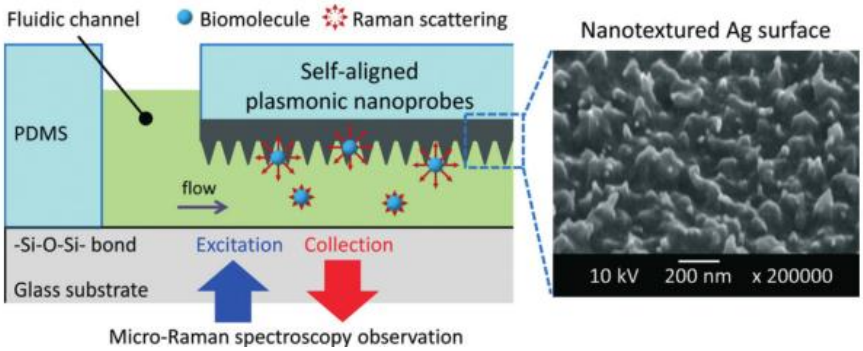

Figure 1.1 Self-alignment of silver nanoparticles on the PDMS surface and the insert is an SEM image of the surface of silver nanoparticles, reproduced from [19].

Although plasma treatment could enhance sensitivity of SERS signal, nanotips and nanorods were randomly generated. The size and shape of the nanotips and nanorods were not uniform, which could lead to poor reproducibility of SERS signal. Accordingly, the quality of hotspots on SERS substrates would play an important role for SERS measurements.

Generally, SERS substrates are usually made from noble metals, such as Ag and Au. The substrates could be categorized into two groups; the first group is nanocolloids and the other is mesoporous materials [20]. The hotspots of nanocolloids are generated at the interconnection between the two adjacent nanocolloidals particles. When electrons on the surface of nanocolloids are exposed to an incident light, the localized surface plasmon resonance (LSPR) occurs, causing constructive interference of the electric field at the interconnected particles [21, 22]. At this area, the intensity of an incident light is intensed, which is called hotspots. Examples of using microfluidic systems for the synthesis of nanocolloids to be used as on-chip SERS substrates are shown by the following works.

Tong and coworkers [23] reported the use of a Y-shaped channel for an in-channel microfluidic mixing. Results showed that complete mixing between analytes and Ag nanocolloids was obtained within 6 min. The device was applied for determination of thiophenol and 2-naphthalenethiol and demonstrated the ease of solution switching between different analytes for multipurpose assays. Moreover,

nanocolloids-based SERS detection coupled with segmented flow or droplet-based microfluidics, which provides the advantage of high-throughput analysis, was also reported [14, 24, 25].

Gao and coworker [14] proposed an in-situ system for synthesis of Ag nonocolloids as on-chip SERS substrates for on-chip determination of diaquat dibromide monohydrate in water. In this work, Ag nanocolloids were synthesized using a droplet-based microfluidic system. The device composed of two parts, the first part was for the synthesis of Ag nanoparticles. Reagents including $AgNO_3$, hydroxylamine hydrochloride and sodium hydroxide were mixed in the droplets and moved along the micochannel **Fig. 1.2(a)**. SEM images showed that Ag nanoparticles were grown along the channel **Fig. 1.2(b)**. Averageded particle size of the obtained Ag nanoparticle was found to be 200 nm with a narrow size distribution. The second part of the device was for the detection of diaquat dibromide monohydrate. The droplets from the first part of the device containing Ag nanoparticles were merged with the analyte solution from the second part of the device, as shown in **Fig. 1.2(c)**. SERS signals were collected after the Ag nanoparticles mixed with the analyte. Results showed high sensitivity with LOD below 5 μM and the droplet-based microfluidic system also provided a high-through platform for highly reproducible synthesis of Ag nanoparticles.

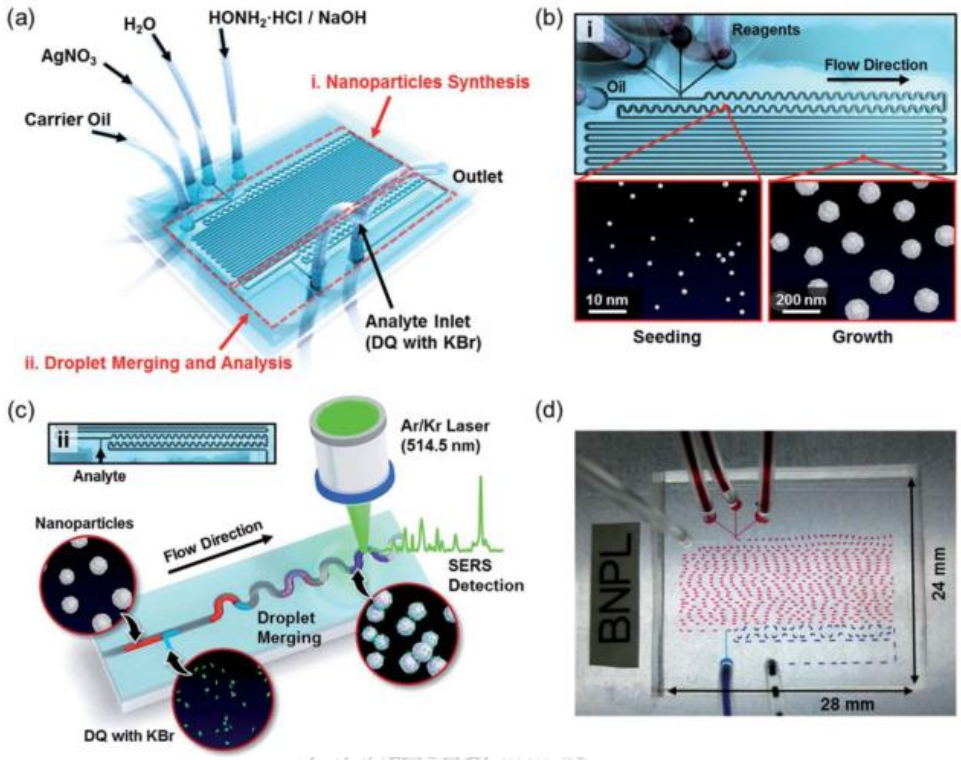

Figure 1.2 (a) A microfluidic device for synthesis of Ag nanoparticles, (b) SEM images of Ag nanoparticles at different points from the inlet, (c) droplet merging between droplets containing Ag nanoparticles and the analyte solution and (d) the size of the device (28×24 mm), reproduced from [14].

Parisi and coworkers [21] reported in situ synthesis of silver nanoparticles (AgNPs) decorated vertical nanowalls as SERs substrates for in-channel sensing. In-channel three pre-patterned electrodes; Co, Ti and Pt as working, counter and reference electrodes, respectively, were designed, as shown in **Fig. 1.3**.

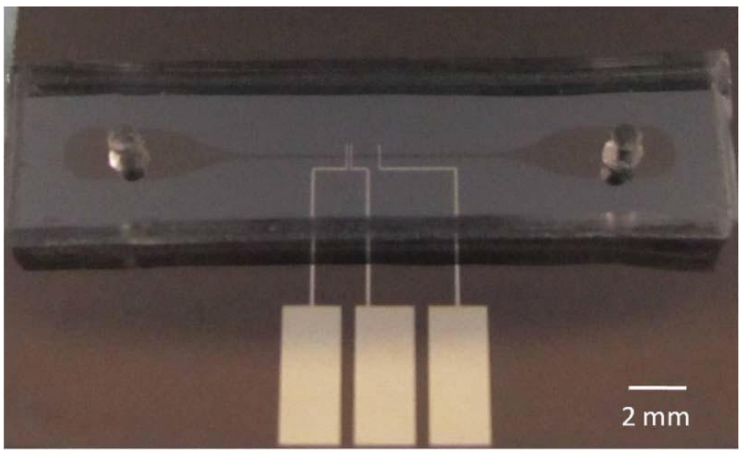

Figure 1.3 In-channel three pre-patterned electrodes for synthesis of silver nanoparticles (AgNPs), reproduced from [21].

The AgNPs were synthesized using two steps. The first step was to deposit Cu on the electrode surface. A constant potential of 22.7 V was applied to the working electrode while the mixture of 0.015 M copper(II) acetate hydrate ($Cu(OAc)_2$) and 0.009 M cetyltrimethylammonium bromide (CTAB) was pumped through. Followed by galvanic replacement of Cu with Ag^+ by flowing $AgNO_3$ solution through the microchannel, AgNPs were generated and deposited on the surface of microelectrodes in the microchannel, as shown in **Fig. 1.4**. These synthesized AgNPs were used as SERS substrates for detection of crystal violet in the PDMS microfluidic device. The approach showed highly analytical performance with low detection limit of 50 pM. The enrichment factor was found to be 1.1×10^9.

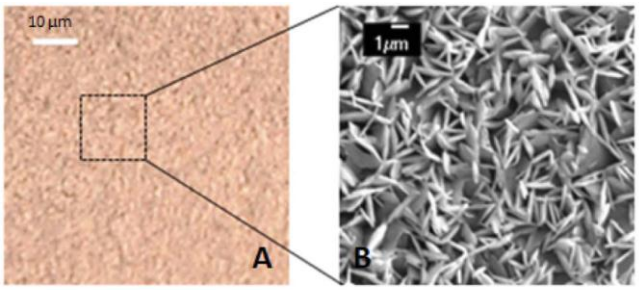

Figure 1.4 (a) Digital and (b) SEM images of nanowalls grown on the working electrode, reproduced from [21].

However, a drawback of nanocolloids is that SRES signal from this type of hotspots is uncontrollable because nanocolloids are randomly aggregated [20], leading to the lack of reproducibility of SERS signal. The other type of SERS substrate is a plasmonic material or mesoporous material or porous like material. Noble metals, such as gold and silver are commonly used to synthesize mesoporous SERS substrates. This material is in a solid state with the size of micrometer. The surface of this material is covered with continuous pores in nanometer sizes, which is LSPR active. This material provides a constant distance of the interconnected particles which is also called interconnected grain sizes. Therefore, this type of materials provides static hotspots which could be more reproducible SERS signal compared to SERS signal from dynamic hotspots. As mentioned that the size of mesoporous materials is in micrometer, mesoporous materials are easily focused under an optical microscope, which is very compatible with microfluidics because, in microfluidic systems, experiments are mostly preformed under an inverted microscope. Mesoporous materials can be easily observable and traceable during the experiments occurring in a microfluidic device. Therefore, a mesoporous material is a good choice to be used as an on-chip SERS substrate compared to nanocolloids which cannot be focused under normal magnification of an optical microscope. However, from the literature reviews, synthesis of mesoporous SRES substrates in microfluidic systems has not yet been reported. The recent work of using mesoporous SERS substrates in a microfluidic system was reported as the following literature.

Mettela and coworkers [26] reported the use of Ag microflowers as manipulable and reusable SERS substrates in a microfluidic device. Ag microflowers were synthesized off-chip (batch synthesis) using a two-step chemical process. The first step was to generate AgBr microflowers using thermolysis of silver tetraoctylammonium bromide (AgToABr) at 250 ºC. The obtained AgBr microflowers with 3 to 6 branches had the overall size of approximately 50-100 µm and the surface was smooth without pores. Followed by chemical reduction of AgBr using $NaBH_4$ solution, Ag nanopaticles with interconnected pores of 25-40 nm were formed, as shown in **Fig. 1.5**. The synthesis of Ag nanoparticles required very small volume (nanoliters) of solutions.

Moreover, these particles were reused by wet chemical cleaning over multiple cycles. In this work, an Ag microflower was successfully used as a single particle SERS substrate for determination of thiophenol (a test analyte) in a microfluidic device (**Fig.1.6**). Results showed uniform SERS enhancement factors in the range of 10^6-10^8. In addition, the Ag microflowers were used for labeled and label-free detection of DNA.

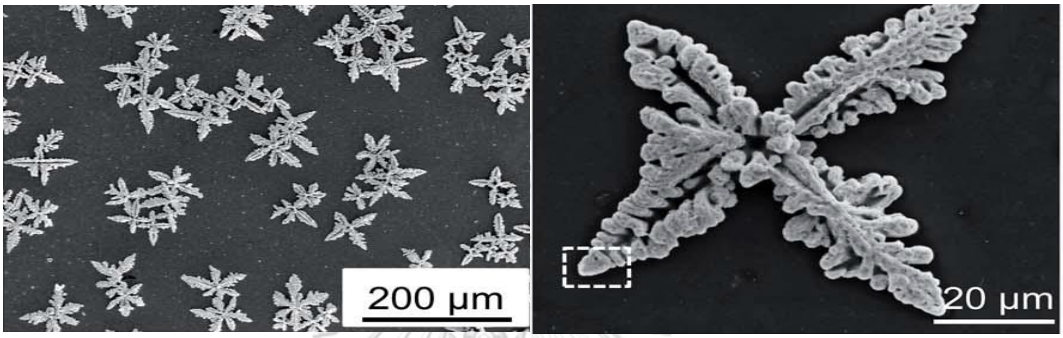

Figure 1.5 Ag microflowers (after $NaBH_4$ reduction) with different magnifications, reproduced from [26].

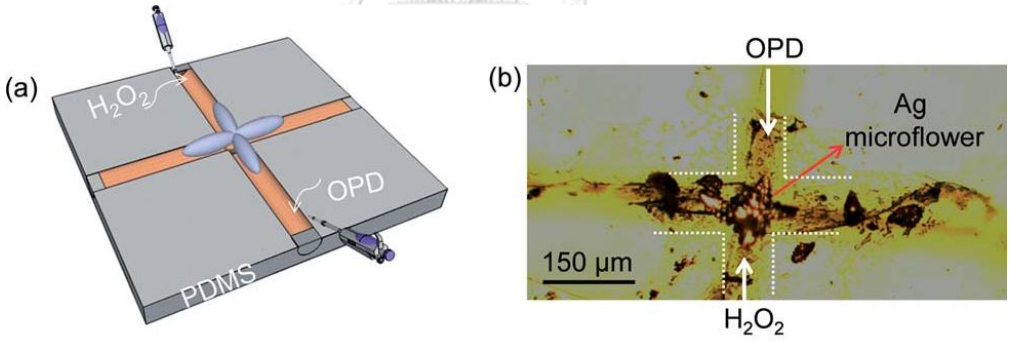

Figure 1.6 (a) A schematic of a microfluidic device with an Ag microflower embedded in the microchannel (b) An optical image of the Ag microflower embedded in a microfluidic channel, reproduced from [26].

As seen from the previous examples, the use of nanoporous microstructures (np-MSs) embedded in a microfluidic channel could enhance analytical performance of SERS detection. Moreover, np-MSs provide identically controllable SERS-active sites, resulting in more reproducible SERS signal. Due to large particle size of np-MSs, it is easily to be manipulated and focused under a microscope. In addition, noble metal

np-MSs can be reused several times using chemical re-generation [27]. Although, from the literature review, thermolysis used in Mettela's work [26] could manipulate the structure of AgBr templates, high temperature could lead to oxide formation on the particle surface [28]. Moreover, using high temperature is not compatible with PDMS microfluidic devices.

Recently, a simple method for the synthesis of nanoporous Ag microstructures (np-AgMSs) was reported [27]. The synthesis condition is mild and simple . Moreover, the method does not involve in temperature or surfactant. Therefore, the synthesized particles would have clean surface. Details of the synthesis is explained in details as the following literature.

In 2015, Wongravee and coworkers [27] reported the use of nanoporous Ag microstructures (np-AgMSs) to be used as a single particle for SERS detection. The np-AgMSs which were mesoporous materials were fabricated using Cl^- induced precipitation of $Ag(NH_3)_2^+$ followed by galvanic replacement of the fabricated AgCl to form Ag^0 or np-AgMSs with a symmetric hexapod structure. Zn metal was used as the sacrificed metal. An chemical equation of the synthesis is shown in Equation 1.1.

$$[Ag(NH_3)]^+_{(aq)} + Cl^-_{(aq)} + H_2O_{(l)} \xrightarrow{Zn} AgCl_{(s)} + NH_4OH_{(aq)} \qquad (1.1)$$

The synthesized np-AgMSs characterized by SEM were found to be a hexapod structure with a uniform pore size of approximately 60 nm, as shown in **Fig. 1.7**. The SERS enhancement efficiency of np-AgMSs was investigated using *p*-aminothiophenol (PATP) as an analyte. Results showed reproducible SERS signal with linearity in the range of 10^{-8}-10^{-3} M. Moreover, the np-AgMSs were reused by chemical regeneration for several cycles without significant decrease in SERS signal.

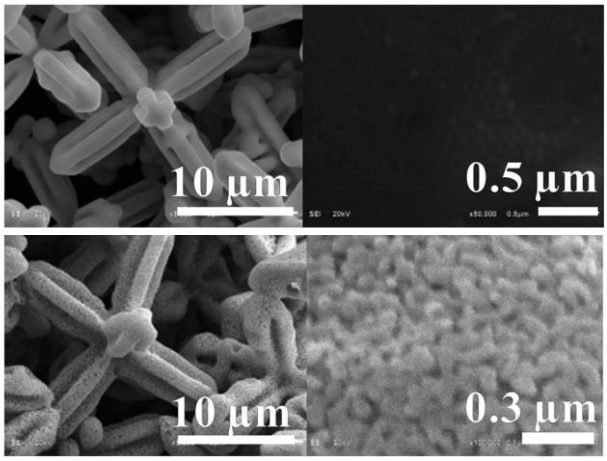

Figure 1.7 Low and high magnifications of SEM micrographs of (a) hexapod AgCl and (b) nanoporous Ag microstructures, reproduced from [27].

However, the work of Wongravee and coworkers [27] only illustrated the SERS ability of np-AgMSs using PATP which is a common Raman active compound. In the present work, we were interested in using np-AgMSs as SERS substrates for determination of glutathione (GSH) which is an organic compound. A microfluidic device was chosen as a platform for the analysis. Using a microfluidic device, np-AgMSs were embedded onto the microchannel surface, which made the particle to be easily manipulated. Therefore, in the first part of our work, we were focused on the use of np-AgMSs, which were off-chip synthesized, as on-chip SERS substrates for determination of GSH using SERS measurements. GSH is an important antioxidant which can prevent damage to important cellular components, which is caused by reactive oxygen species, such as free radicals, peroxides, lipid peroxides and heavy metals [29]. Due to low SERS signal of GSH, there was a previous publication reporting the use of rhodamine 6G (R6G) as a reversed reporting agent for SERS measurements of GSH [30]. As an organic dye, R6G capped on the np-AgMSs surface provided high SERS signal. However, the SERS signal of R6G was decreased in the presence of GSH having a thiol group which strongly bound to the surface of the np-AgMSs. The decrease of the SERS signal was monitored with respect to the amount of GSH. In the present work, we introduced the SERS technique for detection of GSH using a microfluidic system, which could provide high sensitivity, online detection and easy manipulation. In addition,

analysis using a microfluidic system combined with SERS detection could be possibly performed in a high-throughput manner.

As mentioned earlier, on-chip synthesis of np-MSs has not yet been reported. Most of the works on on-chip nanosynthesis were related to nanocolloids with simple structures. However, a synthesis method for fabrication of np-AgMSs, which was recently reported by Wongravee and coworkers [27], was a very simple approach. This system could be compatible with microfluidic synthesis. On-chip synthesis provides advantages over batch synthesis in terms of batch-to-batch reproducibility. In batch synthesis, many factors are needed to be precisely controlled, such as; mixing rate, order of mixing of reactants, temperature, reagent concentration and reaction time. Otherwise, the results could end up with large batch-to-batch variation of nanoparticles properties. Moreover, in a batch synthesis system, the reagents have to be freshly prepared or diluted form stock solutions and the synthesis is repeated all over again to optimize the condition for a desired product. However, in microfluidic systems, reactant concentration can be easily changed by changing input flow rates. By taking this advantage, microfluidic systems can be used to preform screening experiments in order to study the effect of reactant concentration on the structure of nanoparticles.

Therefore, in the second part, we focused on the synthesis of np-AgMSs using a microfluidic system. The synthesis method followed the approach previously proposed by Wongravee and coworkers [27]. Effects of reactant concentration were studied by systematically adjusting the reactant flow rates. The synthesized np-AgMSs were used as on-chip SERS substrates for determination of thiocyanate (SCN^-) in saliva.

1.3 Objectives of This Work

1. To use np-AgMSs synthesized off-chip to be as on-chip SERS substrates for determination of GSH.

2. To develop a microfluidic system as an on-chip microreactor for synthesis of np-AgMSs to be used as SERS substrates for on-chip determination of SCN^- in saliva.

1.4 Scope of This Work

Scope of this work is to develop microfluidic-SERS integrated systems for on-chip detection of GSH and SCN^-.

For determination of GSH, indirect detection or a reversed reporting method was applied using R6G as a Raman reporter. np-AgMSs were synthesized off-chip to be used as SERS substrates. The np-AgMSs were embedded onto the microchannel surface. R6G solution was pumped into the microchannel to bond with the embedded np-AgMSs. Then SERS signal of R6G-np-AgMSs was collected. After that, GSH solution was pumped into the same microfluidic device. R6G was replaced by GSH molecules causing the decrease in the number of R6G-np-AgMSs. Therefore the obtained SERS signal was decreased which corresponded to the GSH concentration. Normalized intensity of the decreased SERS signal were calculated and used for constructed the calibration curve. The analytical performance of this method for determination of GSH, including linearity, limit of detection (LOD) and limit of quantitation (LOQ), was studied.

Furthermore, another microfluidic system was developed for on-chip synthesis of np-AgMSs. Then, the synthesized np-AgMSs were characterized using SEM/EDS and used as on-chip SERS substrates for determination of SCN^- in saliva. For the synthesis part, Cl^- induced precipitation of $Ag(NH_3)_2^+$ coupled with chemical reduction was used. Effect of concentration on the synthesized particle was studied by changing the input flow rates of reactants. The ability of np-AgMSs as SERS substrates was tested using 10^{-5} M PATP as a model analyte. Then, the developed system was used for determination of SCN^- in saliva. The analytical performance of the system was studied, including linearity, LOD, LOQ, interday and intraday precisions, and accuracy.

CHAPTER II
THEORY

2.1 Surface Enhance Raman Scattering (SERS)

Raman is a spectroscopy technique to observe the change in polarization of electron cloud around an analyte molecule, which is caused by vibrational, rotational, and other low-frequency modes [31, 32]. Raman spectroscopy is an alternative technique for detection of organic molecules. The Raman technique has advantages, such as low operation cost, fast detection, labeled-free detection and non-invasive technique [33]. Raman also offer very high specificity because inelastic vibration, including stoke and anti-stoke (**Fig. 2.1**) proving a specifically spectral shift for individual molecule [33]. Therefore, sample preparation is rarely required or no sample preparation is needed because this technique provides fingerprints for specific molecules [21, 22]. The major advantage of Raman spectroscopy over IR spectroscopy is that a water molecule is not Raman active [18] because water is a highly asymmetric molecule and its vibrational mode does not change the polarizability of the molecule. Therefore, Raman signal of samples can be measured in aqueous media [33]. However, sensitivity of Raman spectroscopy is quite poor because Raman scattering light emitting from analyte molecules after being excited by the incident light is quite low. To improve the sensitivity of Raman spectroscopy, surface enhance Raman scattering (SERS) has been used to compensate the problem by enhancing the incident light intensity using noble metal nanoparticles as SERS substrates [34]. The sensitivity of SERS can be improved up to 10^{14} orders of magnitude compared to those of conventional Raman spectroscopy [16]. Surface to volume ratios of noble metals, such as Ag, Au and Pt are increased significantly when the particle size is down to 1-100 nm. When nanoparticles are being exposed to an incident light, electrons on the particle surface are oscillated with the electromagnetic light (**Fig. 2.2(a)**), causing constructive interference at the interconnected particles via localized surface Plasmon resonance (LSPR) phenomena [20, 35]. At the interconnected area, highly intensed electromagnetic field is observed. This area is also called a hotspot. An analyte

molecule which is located at the hotspot area is exposed to the highly intensed electric field. Consequently, there are a lot of electrons at the excited state. Therefore, signal form Raman scattering is massively improved.

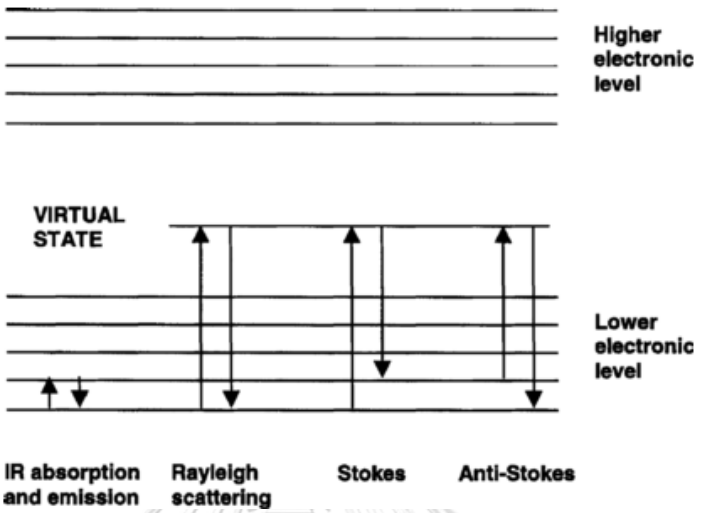

Figure 2.1 Schematic representation of energy transitions in IR and Raman spectroscopy, reproduced from [33].

2.2 SERS Substrate

Although SERS can enhance sensitivity of conventional Raman spectroscopy, the sensitivity and reproducibility of SERS signal are strongly related to the quality of hotspots on a SERS substrate [36]. Nanocolloids are common SERS substrates which can be synthesized by both top-down and bottom-up approaches [37]. Hotspots of nanocolloids are generated at the distance between the two adjacent particles of nanocolloids (**Fig. 2.2(b)**), which is stabilized under electromagnetic interaction of ionic stabilizer [35, 38, 39]. An analyte molecule which is located at the hotspot area is exposed to highly intensed electric field, causing enhancement of Raman scattering light, as shown in **Fig. 2.3**. The distance between nanoparticles directly affects SERS enhancement. The shorter distance provides the grater enhancement factor of SERS signal, as shown in **Fig. 2.2(c)**. The disadvantage of nanocolloids is an uncontrollable hotspot size due to random aggregation of nanoparticles, [20]. Therefore, the size of dynamic hotspots is changed along with the particle movement, which could lead to poor reproducibility of SERS signal [20].

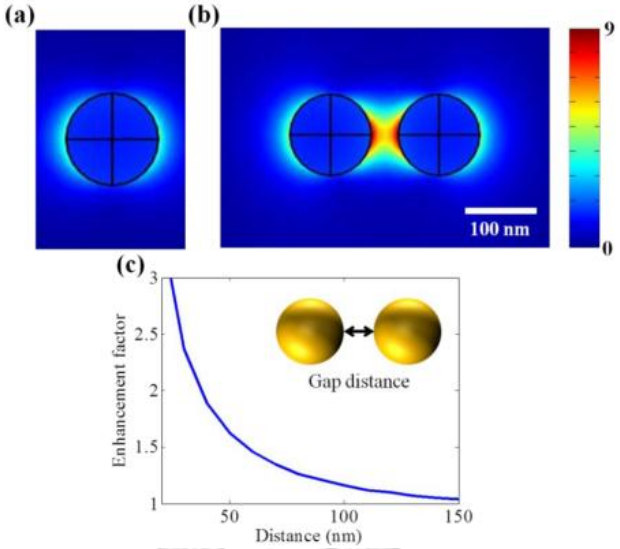

Figure 2.2 (a) Oscillation of electron cloud on the nanoparticle surface under LSPR during being exposed to an incident light, (b) constructive interference of electrons between two nanoparticles and (c) the correlation between distance between the two nanoparticles and enhancement factor of SERS signal, reproduced from [40].

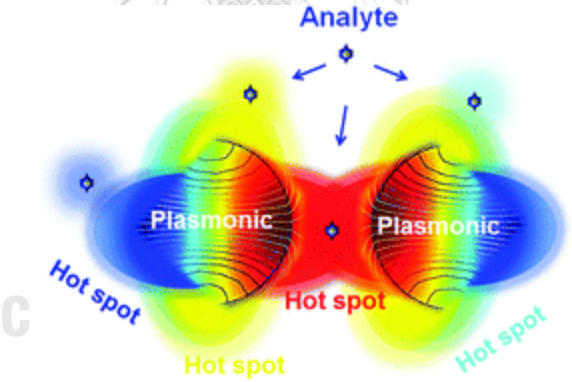

Figure 2.3 An analyte molecule on a hotspot area of nanocolloids is exposed to highly intense electric field [41].

The other type of hotspots besides nanocolloids is static hotspots generated from mesoporous, porous-like materials or plasmonic materials [42]. These materials are in solid form which has the size in a micrometer scale. In addition, there are nanopores covering all over the material surface, which act as hotspots (**Fig. 2.4**). The size of hotspots is constant and corresponds to the interconnected grain particle size [43]. This type of hotspots provides more reproducible SERS signal compared to the aggregated nanocolloids [44]. Moreover, the particle size in micrometer make the particles to be easily focused under a normal microscope. SERS sensitivity strongly depends on the optical properties of metal nanoparticles which are size, shape, arrangement and dielectric environment [45]. Au (gold), Ag (silver) and Cu (cupper) are noble metals which can be used as SERS substrates [46]. However, Au and Ag are the common metals because they are air stable, while Cu is more reactive [46]. To maximize the sensitivity of SERS signal, excitation wavelength which is matched with the adsorption range of the noble metals is chosen. For Ag nanoparticles, an excitation wavelength to provide maximum enhancement is between 500 nm to 600 nm [45]. For Au and Cu, excitation wavelength in the range of 550-1250 nm can be used, as shown in **Fig. 2.5** [46]. In this work, Ag noble metal was chosen because it is compatible with a 532 nm excitation laser which offers higher excitation energy compared to the other excitation wavelength which could lead to higher sensitivity of SERS signal.

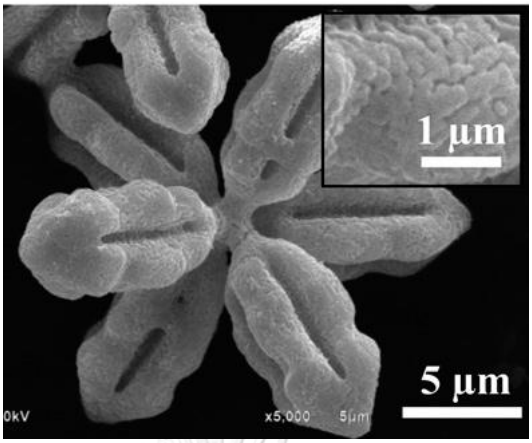

Figure 2.4 A mesoporous material with nanopores covering all over the particle surface, reproduced from [47].

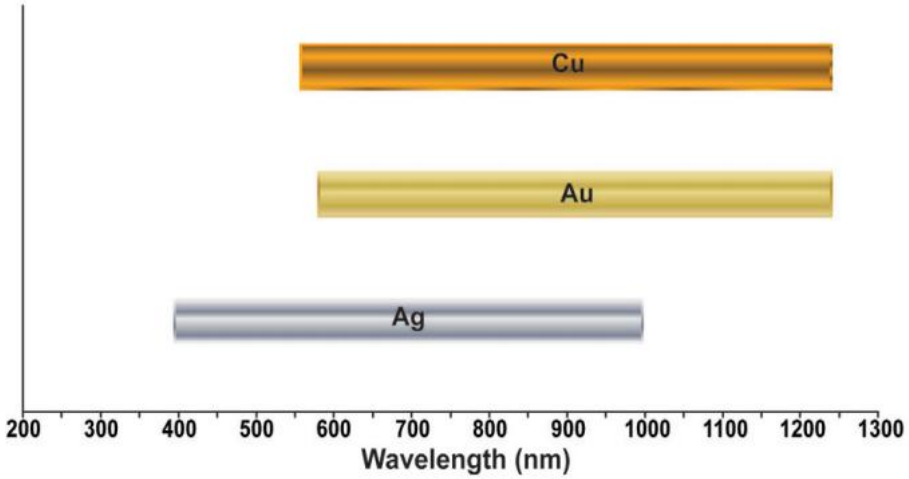

Figure 2.5 Excitation wavelengths that could be used as incident light sources for each noble metal used as a SERS substrate, including Ag, Au and Cu, Reproduce from [46].

2.3 Synthesis of Nanoporous Ag Microstructures (np-AgMSs)

A template method is commonly used to synthesize np-AgMSs [42]. The synthesis starts with fabrication of a silver salt template, such as AgCl or AgBr. The synthesis uses $AgNO_3$ to react with a simple salt, such as NaCl or NaBr to form AgCl or AgBr, respectively. Generally, AgCl and AgBr arrange itself into a cubic structure ((110)

facet) which is the lowest energy surface [48, 49]. This growth mechanism is a thermodynamic control to preserve the lowest total energy of the system [50].

To manipulate the structure of a silver salt, several methods have been used. For example, AgBr particles were thermalized at 250 °C for 1 h in air. The structure of AgBr changed from cubic to microflower [51], as shown in **Fig. 2.6**.

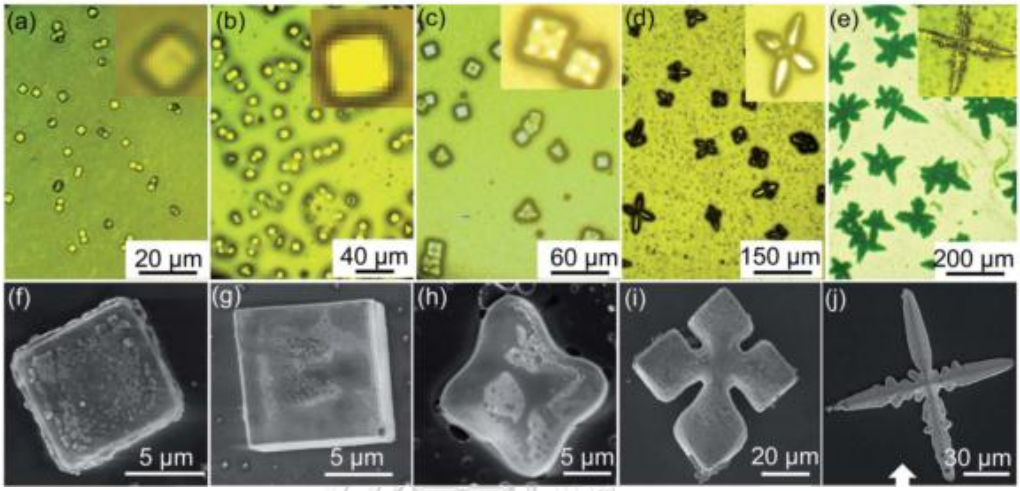

Figure 2.6 Microscope images (a-e) and SEM images (f-g) of the synthesized AgBr microparticles. (a-e) and (f-g) showed structure development of AgBr from cubic to microflower, reproduced from [51].

However, the use of high temperature can lead to impure materials caused by the formation of oxide layer on the particle surface [28]. For milder conditions to control the structure of silver salt particles, shape controlling agents or chemical reagents, such as NH_4OH [47], poly(vinyl pyrrolidone) [52], surfactant [52] and H_2O_2 [53], are used. NH_4OH was chosen as a shape controlling agent for the synthesis of AgCl microstructures because it provided clean surface of materials [47]. NH_4OH causes a selective dissolution of <111> which is the corners of the cubic seed. Therefore, a cubic seed is turned into an octahedral seed. Then, the corner of the octahedral seed is grown faster compared to edge and facet. Consequently, an octahedral seed is grown into a hexapod AgCl structure.

Two different methods can be used to transform silver salt templates into zerovalent silver mesoporous materials. The first method is galvanization using a metal

plate, such as Zn, Cu or Al, as a sacrificial metal. Due to high reduction potential of Ag^+ (E^0 of $Ag^+ \longrightarrow Ag^0$ in water = +0.79 V) [54]), several metals can be chosen as a sacrificial metal to provide an electron to a silver ion [55]. Galvanization time is depended on the type of the sacrificial metal. However, this method is time consuming. The other method is a chemical reduction, $NaBH_4$ is a strong reducing agent used to reduce Ag^+ to form Ag^0. The reaction occurs instantly and the particles can retain the same silver salt structure [28, 51]. Besides $NaBH_4$, another reducing agent could be used, such as L-ascorbic acid [55].

Although batch synthesis provides a simple setup for synthesis of mesoporous materials, poor mass and heat transfer could lead to variation of the obtain product in terms of size, shape and SERS property. Microfluidic systems have been wildly used as microreactors for synthesis due to great mass and heat transfer of reactants in microchannels. Using microfluidic systems could provide high reproducibility of the synthesized materials.

2.4 Synthesis in Microfluidic Systems

Lab on a chip or microfluidics is the system which manipulates liquid in a small channel having dimensions in micrometers [56]. A microfluidic device is generally made from polydimethyl siloxane (PDMS), but occasionally made from glass for specific applications. Lab on a chip can be categorized as a miniaturized system which combines the laboratory processes, including sample preparation, pre-concentration, chemical reaction and detection into a single device [56]. Microfluidic systems are commonly used as analytical devices for a variety of applications, such as chemistry, biology, environment and point-of care (POC) diagnostics [1-4]. Apart from analytical applications, microfluidic systems are used as microreactors for the synthesis purpose.

Microfluidic systems handle small fluid volumes down to nano or picoliters [17, 57]. Therefore, mass and heat transfer are improved which could improve the rate of reaction and more reproducible result could be obtained compared to batch systems [17, 57]. Moreover, microfluidic systems provide several advantages for the synthesis, such as small reactant volume, continuous system and possibly automated systems

[8]. Moreover, the reactants concentration in microchannel can be adjusted easily by changing the input flow rates [8]. By taking the advantage of good mass and heat transfer, microfluidic systems can be used as microreactors for synthesis applications, especially the synthesis of nanoparticles which is required narrow size distribution and high reproducibility of the particles [11-13]. To increase mixing rate of reactants in microchannels, several configurations of microchannal are applied for the synthesis, such as T-shape, Zigzag-shaped, 3-D-L-shaped, 3-D connected out-of-plane, and Staggered-herringbone grooves [58], as shown in Fig. 2.7.

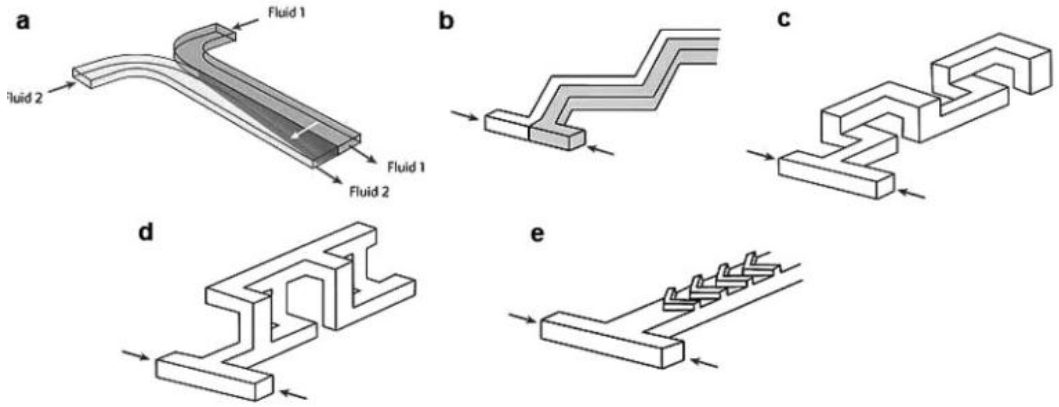

Figure 2.7 Different configurations of microfluidic channels for the synthesis of SERS substrates (a) T-shape, (b) Zigzag-shaped, (c) 3-D-L-shaped, (d) 3-D connected out-of-plane and (e) Staggered-herringbone grooves. Reproduced from [58].

A flow-focusing microchannel (Fig. 2.8) is one of the powerful configurations which provide fast mixing because this configuration could reduce the diffusion distance between two reactants [9]. This configuration provides faster mixing rate compared to a normal T-junction configuration. Consequently, the obtained products would be more reproducible.

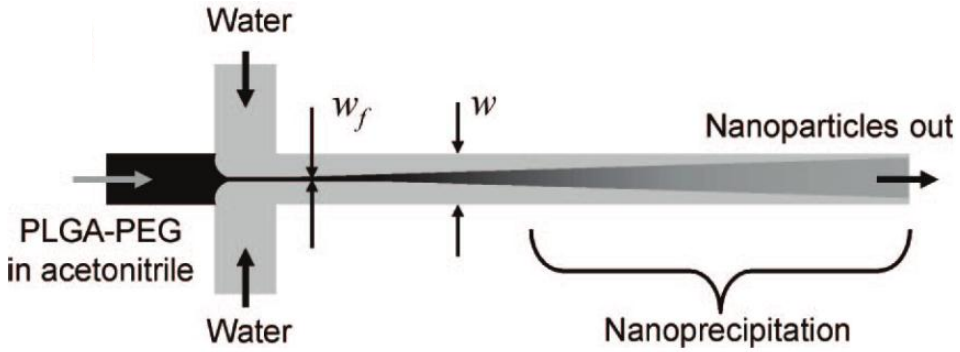

Figure 2.8 The use of flow-focusing microfluidics for nanoparticle synthesis. Reproduced from [9].

Several procedures have synthesized SERS substrates using microfluidic systems [14, 21-24, 35, 59, 60], such as, deposition of silver metal thin film onto a microfluidic channel followed with surface modification to generate rough surface using oxygen plasma treatment [19], electrochemical reduction of silver ion to create nanoparticle of Ag^0 [21] and the simple method of chemical reduction of silver ion to form Ag^0 nanocolloids [16].

2.5 Microfluidics Coupled with SERS Detection

According to small volumes in microfluidic systems, a highly sensitive detection system is required. Fluorescence is the most common detector used in microfluidic systems. However, for detection of non-fluorescence analytes, a fluorescence dye for molecule tagging is required [11]. Moreover, fluorescence lacks structural information of analytes [11]. Besides fluorescence, SERS is one of the highly sensitive spectroscopic techniques which provides specifically a spectral shift for an individual molecule without special treatment of analytes. SERS detection is also compatible with microfluidic systems because PDMS which is a material for microfluidic device is Raman inactive. Therefore, spectral shift of PDMS is not shown in SERS spectra. However, to increase Raman sensitivity, high quality SERS substrates are required. The role of SERS substrates is to enhance intensity of an incident light. To synthesize SERS substrates, a microfluidic system can be used as an on-chip microreactor. Reactant concentrations in microlfluidic systems can be manipulated by changing the input flow rates. Several publications have been reported on the use of microfluidics for the synthesis of SERS

substrates and continuous use–for on-chip determination of Raman active analytes [11, 14, 21, 23, 24] as shown in Fig. 2.10. SERS substrates can be synthesized by several approaches, such as sol-gel [61], electrochemistry [21, 62] and growth in porous membranes [63]. The synthesized SERS substrates were used for on-chip detection of SERS active compounds, such as rhodamine 6G [22], malachite green isothiocyanate [15], ochratoxin A [64], carbendazim [22, 35], thiocyanate [65], adenosine [66], crystal violet [61] and dopamine [19]. Combination of microfluidic-SERS detection provides advantages of high-throughput analysis, reproducibility and easy manipulateion of nanoparticles.

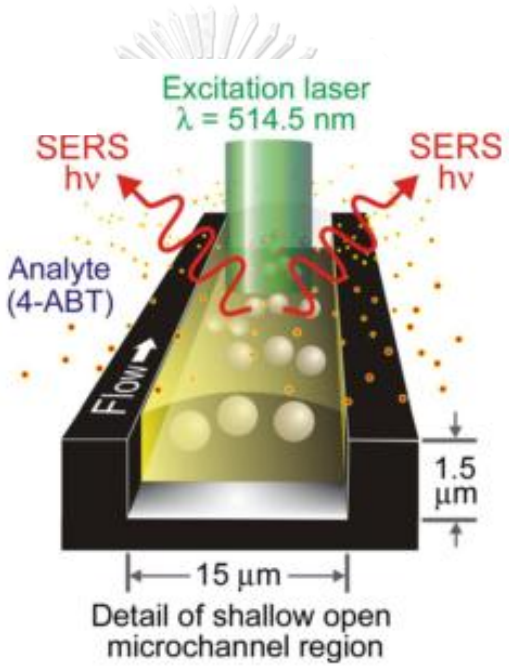

Figure 2.9 On-chip synthesis of SERS substrates which were continuously used as on-chip SERS substrates for the determination of analyte, reproduced from [67].

CHAPTER III

EXPERIMENTAL

3.1 Instruments and Equipment

Table 3.1 List of instruments and equipments.

Instruments and equipment	Companies
1. Micropipette (10, 100 and 1,000 µL)	Eppendorf (Thailand)
2. Safe-lock tubes (1.5 mL)	Eppendorf (Thailand)
3. Analytical balance (5 digit)	Mettler (Canada)
4. Volumetric flask	PVG International (India)
5. Puncher (8 mm diameter)	Robbins Instruments, Inc. (USA)
6. Syringe pump	Harvard apparatus (Thailand)
7. Syringe needle	NIPRO (Thailand)
8. UV curing chamber	Uvitron international (USA)
9. Spin-coater	Specialty coating system (USA)
10. Oven	Memmert (Germany)
11. CO_2 laser cutter	DHM laser & cutting (China)
12. DXR Raman spectroscopy	Thermo scientific (Thailand)
13. Scanning electron microscope coupled with energy dispersive X-ray spectroscopy (SEM/EDS), JEOL JSM-6510A	Thermo scientific (Thailand)
14. Optical inverted microscope	Vision DX 16, Bara vision engineering (Thailand)

3.2 Chemicals

Table 3.2 List of chemicals.

Chemicals	Companies
1. Rhodamine 6G (R6G)	Sigma Aldrich (Singapore)
2. Glutathione (GSH)	Sigma Aldrich (Singapore)
3. Silver nitrate ($AgNO_3$)	Merck (Germany)
4. Sodium borohydride ($NaBH_4$)	Merck (Germany)
5. Sodium chloride (NaCl)	Merck (Germany)
6. Ammonium hydroxide 25% w/w (NH_4OH)	Merck (Germany)
7. Deionized water (Milli-Q Gradient)	Millipore (Thailand)
8. SU-8 3025	MicroChem (USA)
9. SU-8 developer	MicroChem (USA)
10. SYLGARD® 184 silicone elastomer kit based	Dow corning (Thailand)
11. SYLGARD® 184 silicone curing agent	Dow corning (Thailand)
12. Hydrazine (N_2H_2)	Merck (Germany)
13. Ascorbic acid ($C_6H_8O_6$)	Merck (Germany)
14. Absolute ethanol	Merck (Germany)
15. Potassium thiocyanate (KSCN)	Sigma Aldrich (Singapore)
16. *p*-aminothiophenol (PATP)	Sigma Aldrich (Singapore)
17. Artificial saliva matrix	King Chulalongkorn Memorial Hospital (Thailand)

The experimental section was divided into two parts, the first part was SERS detection of GSH and the second part was on-chip synthesis of np-AgMSs for quantitative determination of SCN^-. However, both parts were shared the same concept of microfluidic systems coupled with Raman detection for chemical/biomedical applications.

3.3 Part I Detection of GSH

3.3.1 Preparation of Nanoporous Silver Microstructures (np-AgMSs)

The approach for synthesis of np-AgMSs followed the method proposed by Gatemala and coworkers. [47, 68] Multipod AgCl templates were off-chip synthesized by mixing 5 mL of 0.1 M $AgNO_3$ with 4.7 mL of 5.31 M NH_4OH. The mixture was poured into 90 mL of 1 M NaCl under vigorously stirring and white precipitation of AgCl was immediately observed. The reaction was stopped after 5 min of the reaction time. The AgCl precipitate was filtrated onto filter paper, then washed using deionized water and then air dried. To create a porous structure, AgCl templates were poured onto 1×1 cm zinc plates in a petri dish. Galvanic reaction between Ag^+ (Ag^+/Ag^0, $E° = -1.8$ V) [69] and Zn^0 (Zn/Zn^{2+}, $E^0 = -0.76$ V) [70] occurred on the metal surface. Ag^+ became Ag^0 by accepting one electron from Zn and then Cl^- was released into the solution. The final product was a porous Ag^0 structure or np-AgMSs. The obtained np-AgMSs were washed using absolute ethanol to remove Cl^- followed with deionized water and air dried. The synthesized np-AgMSs were characterized using SEM. Schematic of the overall synthesis is shown in **Fig. 3.1**.

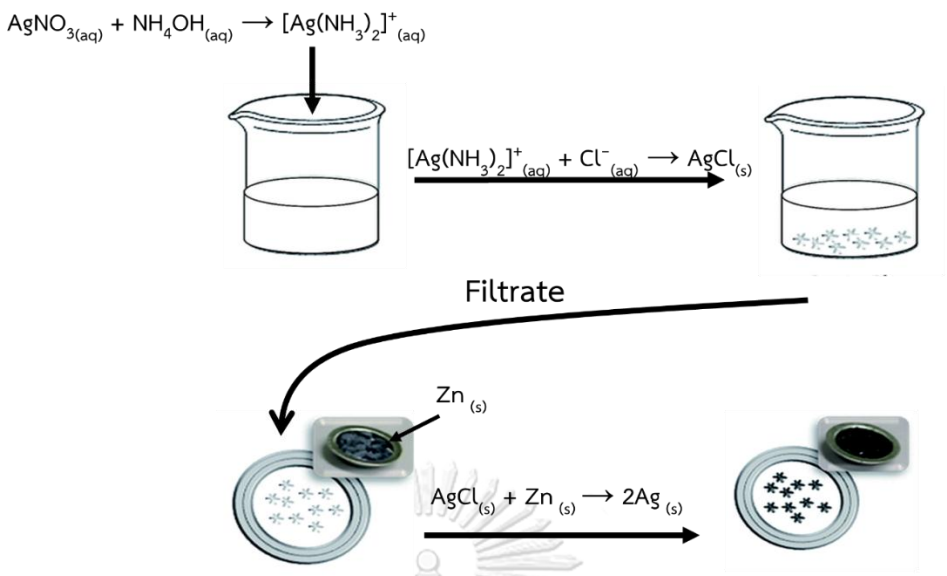

Figure 3.1 Schematic of the synthesis of np-AgMSs, adapted from [27].

3.3.2 Fabrication of Microfluidic Analytical Devices

The layout of a microfluidic device was designed using AutoCAD 2015 program. The design was a cross-channel microfluidic device with 2 inlets for sample and washing solutions and 2 outlets, as shown in **Fig. 3.2(a)**. The center of the cross channel was a detection zone. The channel dimensions were 300 µm wide and 100 µm deep. Polydimethyl siloxane (PDMS) was chosen as a material for device fabrication. The fabrication of PDMS device started with fabricating an SU-8 photoresist mold using soft lithography [71]. The mold was used for PDMS replica. PDMS prepolymer and curing agent were mixed at a ratio of 10:1 w/w and degassed using a vacuum chamber. The mixed solution was poured onto the SU-8 mold and put into an oven at 65 °C for 4 h. The cured PDMS was cut into desired pieces, then peeled from the mold and then punched to make inlet and outlet holes for fluidic access. Subsequently, 100 µl of 0.03 g mL^{-1} of np-AgMSs were drop casted onto the detection area (the center of the cross channel), as shown in **Fig. 3.2(b)**. Finally, the PDMS was enclosed with a glass slide using plasma bonding. Schematic of the device fabrication is shown in **Fig. 3.3**.

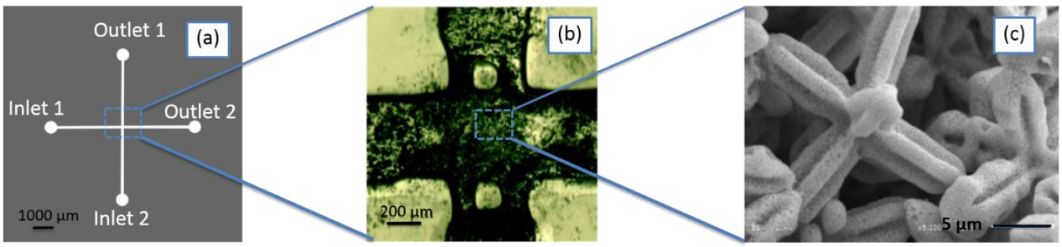

Figure 3.2 (a) Design of microchannels, (b) an microscope image of detection zone with embedded np-AgMs and (c) an SEM image of embedded np-AgMSs (reproduced from [27]).

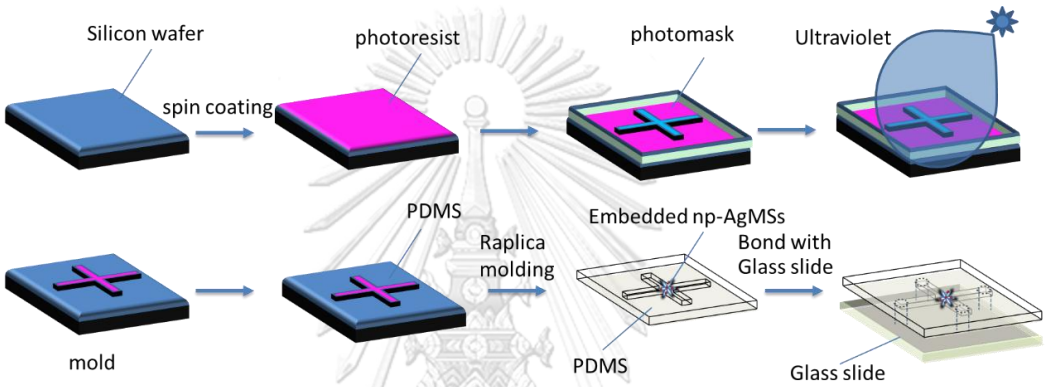

Figure 3.3 Schematic of microfluidic device fabrication using soft lithography.

3.3.3 Effect of Flow Rate on the Embedded np-AgMSs.

The np-AgMSs used as SERS substrates were drop casted onto the center of microchannel. The particles were stuck onto the PDMS surface. However, the particles could be lost under high flow rate conditions. To test the stability of np-AgMSs under flow conditions, Milli Q water was pumped through the microchannel. Different flow rates varied from 0 to 30 µL min^{-1} (flow velocities of 0-16.68 cm^3 s^{-1}) were studied. Subsequently, images of np-AgMSs embedded in the microchannel were taken using an inverted optical microscope with a 10x objective lens.

3.3.4 On-Chip Raman Detection

The first step for detection of GSH was to attach R6G onto the np-AgMSs surface. 10 μM of R6G was loaded into a 1 mL tuberculin syringe with a 0.5×25 mm hypodermic needle and fine bore polythene tubing with an internal diameter of 0.38 mm and external diameter of 1.09 mm. The tubing was connected to standard-pressure infuse/withdraw PHD 2000 syringe pumps. The R6G solution was pumped via inlet no. 1 (Fig. 3.2) using a flow rate of 10 μL min^{-1} for 1 min into the device containing np-AgMSs at the center of the cross channel. The reaction time between R6G and np-AgMSs was studied at 15, 30, 45, 60, 75 and 90 min. SERS spectra of R6G-capped np-AgMSs (R6G-np-AgMSs) were recorded. All SERS-measurements were performed using a DXR Raman microscope. SERS spectra were collected using 32 s irradiation using 1 mW of a 532 nm incident laser under a 10x objective lens coupled with a 25 μm pinhole. The laser beam was focused onto each np-AgMs particle in the microchannel. For each SERS measurement, 20 replicated spectra were acquired from 20 different np-AgMSs particles. The next step was to replace R6G with GSH, which was the analyte. 10^{-5} M of GSH solution was loaded into a 1 mL syringe using the same connection as mentioned above. Then, the GSH solution was pumped into the same inlet using a flow rate of 10 μL min^{-1} for 1 min. The flow was stopped to allow the replacement between GSH and R6G on the np-AgMSs. The incubation time between GSH and R6G-np-AgMSs was studied at 1, 5, 10, 15 and 20 min. The GSH molecules replaced R6G to form a GSH-np-AgMSs complex which was not a Raman active compound. After the incubation, SERS spectra of the remaining R6G-np-AgMSs were collected. Schematic of overall experimental procedure of the reversed reporting technique are shown **in Fig. 3.4**.

3.3.5 Quantitative Analysis

Normalized intensity (I_N) of SERS signal was calculated using **Equation 3.1**;

$$I_N = (I_0-I_1)/I_0 \quad (3.1)$$

where I_0 and I_1 are SERS intensities of the peak at a incubat of R6G-np-AgMSs before and after the addition of GSH, respectively.

To construct a calibration curve, standard solutions of GSH were prepared in the concentration range from 10^{-8} to 10^{-3} M. The calibration curve was plotted between logarithm of GSH concentration and normalized intensity of SERS signal. Lowest of calibration (LOC) was reported.

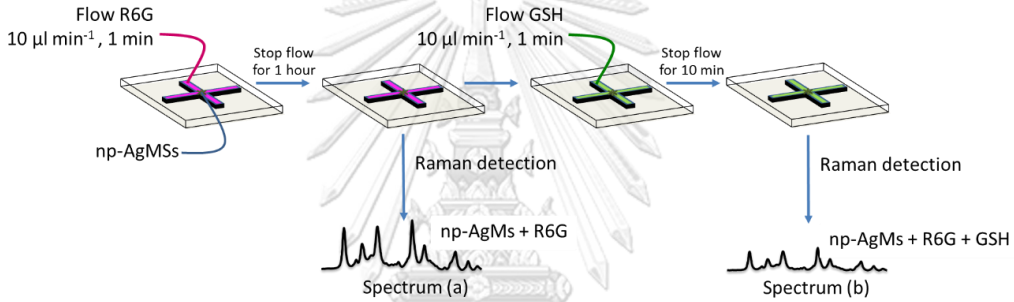

Figure 3.4 Schematic of experimental procedure for determination of GSH using a reversed reporting technique.

3.3.6 Reusability of np-AgMSs SERS Substrate

To test the reusability of np-AgMSs SERS substrates after 1 cycle of SERS detection, chemical regeneration of np-AgMSs using $NaBH_4$ was studied. After SERS spectra were collected, the np-AgMSs were washed using 1 mL of 1 M $NaBH_4$ which is a strong reducing agent. The $NaBH_4$ solution was pumped into the microchannel via inlet no.2 (**Fig. 3.2**) at a flow rate of 10 µL min^{-1} in order to get rid of all organic compounds adsorbed on the np-AgMSs surface. After the np-AgMSs were cleaned, SERS spectra of the cleaned np-AgMSs were re-collected using the same procedure as mentioned in **section 3.3.4**.

3.4. Part II On-chip Synthesis of np-AgMSs as SERS Substrates

3.4.1 Fabrication of Microfluidic Analytical Devices

A flow-focusing microfluidic device was used in this part. The design was drawn using AutoCAD2015 program. Polyvinyl chloride (PVC) sticker was used as a molding material for PDMS replica. PVC sticker was cut into the designed pattern using a CO_2 laser cutter. The design composed of 3 inlets and 1 outlet, as shown in **Fig 3.5 (a)**. All Channel dimensions were 300 µm wide and 100 µm deep. The mixing part which was after the inlets was a 1 cm straight channel, making the overall length of approximately 2 cm. For PDMS replica, the PDMS monomer and curing agent were mixed at a weight ratio of 10:1, degassed and poured into a PVC mold. PDMS was cured at 65 °C in an oven for 3 h, as shown in **Fig. 3.6(a)**. After that, PDMS replica was peeled from the mold and punched holds for fluidic access. Finally, the punched PDMS plate was reversibly bonded with a glass slide using ethanol bonding, as shown in **Fig. 3.6(b)**. Finally, the complete microfluidic device was placed in an oven at 55°C for 2 h.

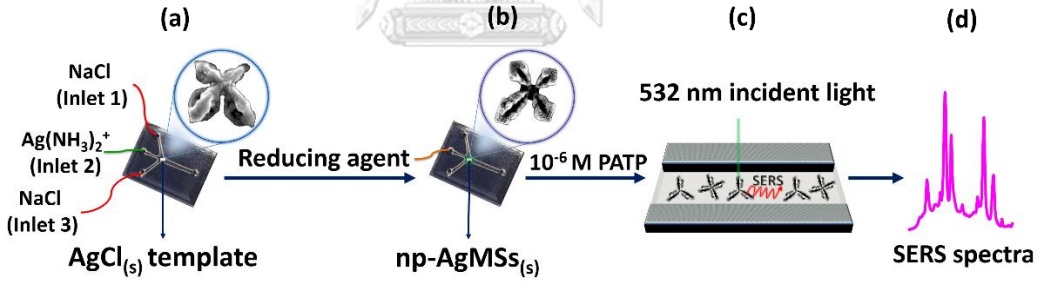

Figure 3.5 Overall experimental setup and procedure; (a) synthesis of AgCl templates, (b) chemical reduction of AgCl to np-AgMSs, (c) SERS detection of PATP using np-AgMSs as SERS substrates and (d) the obtained SERS spectra.

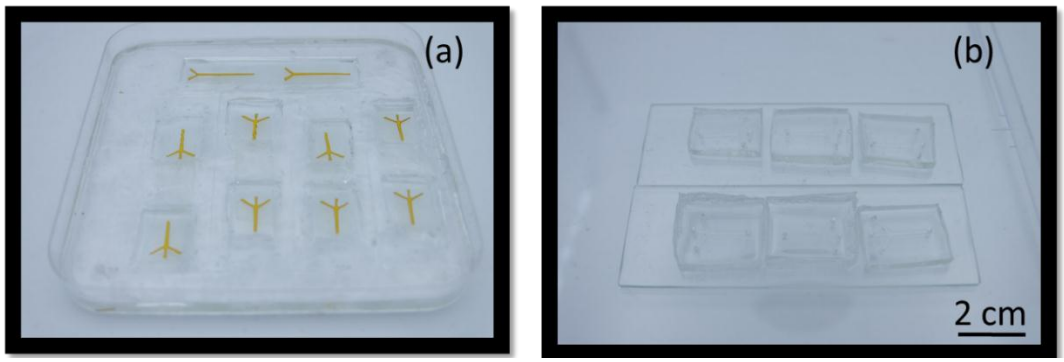

Figure 3.6 (a) PVC sticker was cut as molds for PDMS device fabrication and (b) complete microfluidic devices.

3.4.2 On-chip Synthesis of np-AgMSs

The synthesis of np-AgMSs was divided into two parts; the first part was to synthesize AgCl which was used as a template for fabrication of np-AgMSs. The second part was to chemically reduce the AgCl template to form zerovalent Ag or np-AgMSs. An overall experimental procedure is shown in **Fig. 3.5**.

3.4.2.1 Preparation of AgCl Templates

To synthesize AgCl microstructures as templates for fabrication of np-AgMSs, Cl^- induced precipitation of $Ag(NH_4)_2^+$ was used. The $Ag(NH_4)_2^+$ was prepared off-chip by mixing 1 mL of 0.05 M $AgNO_3$ and 1 mL of 0.15 M NH_4OH. A complex of $Ag(NH_4)_2^+$ occurred with excess NH_4OH leftover in the mixed solution. The solution of $Ag(NH_4)_2^+$ in excess NH_4OH was then loaded into a 1 mL syringe which was connected to the device via the middle inlet. Then, 0.2 M NaCl solution was prepared and loaded into two 1-mL syringes which were connected to the side inlets of the device, as shown in **Fig. 3.5.(a).**

Effects of reactant concentration on the structure of AgCl templates were studied by manipulating the input flow rates without preparing new reactant solutions. It should be noted that the flow rates of side flows were always identical. Therefore, the side flow rate reported in this work represented each side flow. To study the effect of Cl^- concentration, the flow rate of $Ag(NH_4)_2^+$ or the central flow was fixed at 1 μL min^{-1} and the flow rate of Cl^- or side flow was varied from 1 to 2, 4 and

6 μL min^{-1}, corresponding to Exp. (1-4) in Table 3.1, respectively. On the other hand, the effect of NH_4OH concentration was studied by fixing the side flow and increasing the central flow rate from 1 to 2 and 3 μL min^{-1}, corresponding to Exp. (1, 5-6) in Table 3.1, respectively.

Effect of flow velocity or total flow rate on the structure of AgCl templates was also studied. The experiment was performed in two conditions, including high Cl^- and high NH_4OH conditions. For high Cl^- environment, the initial Cl^- concentration of 0.3 M was used instead of 0.2 M. For high NH_4OH environment, the initial NH_4OH concentration of 0.18 M was used instead of 0.15 M. To maintain the reactants concentration, the ratio of the side flow rate to central flow rate was fixed at 2:1 and the total flow rate was increased from 3, 6 and 9 μL min^{-1}, corresponding to flow velocities of 0.17, 0.33 and 0.50 cm min^{-1}, respectively. Details of flow conditions for each experiment are shown in Table 3.1 (Exp. (7-9) for high Cl^- environment and Exp. (10-12) for high NH_4OH environment.

3.4.2.2 Reduction of AgCl Templates

The next step of preparing np-AgMSs was to transform AgCl into zerovalent Ag^0 or np-AgMSs using chemical reduction. Three reducing agents, including concentrated hydrazine, 0.2 M ascorbic acid (pH 8) and 0.2 M sodium borohydride ($NaBH_4$) were prepared. For hydrazine as a reducing agent, 5 μL of concentrated hydrazine was dropped onto a glass slide placed nearby the device in a close plastic box and the reaction was left for 1 night. For ascorbic acid and $NaBH_4$, 5 μL of each solution was directly pipetted into the device containing AgCl templates. After the reduction, 1 mL of NH_4OH was pipetted into the device to clean up all unreduced AgCl and followed by 1 mL of milli Q water twice. Finally, the microfluidic device containing np-AgMSs was placed into an oven at 55 °C for 1 h.

3.4.3 Characterization of AgCl and np-AgMSs

The structure of AgCl templates and np-AgMSs were characterized using an optical inverted microscope with a 40x objective lens coupled with 10x eyes lens. All images from the microscope were processed using the MShort Image analysis system.

To get more structural detail, a scanning electron microscope (SEM) was used. SEM was operated at 20 kV under high vacuum with a secondary electron image (SEI) to obtain high magnification images. Moreover, SEM coupled with energy dispersive X-ray spectroscopy (SEM/EDS) was used to identify the elemental mapping composition for both AgCl templates and np-AgMSs. It should be noted that to calculate the percentage of elements, only Ag and Cl element were taken into consideration.

Table 3.3 Experimental conditions for in situ synthesis of AgCl microstructures.

Exp.	Flow rate ($\mu L\ min^{-1}$)		Final concentration (M)			Ratio	
	$[Ag(NH_3)_2]^+$ central flow	Cl^- side flow	Ag^+	NH_4OH	Cl^-	$[Cl^-]/[Ag^+]$	$[NH_4OH]/[Ag^+]$
1	1	1	0.008	0.025	0.13	16	3
2	1	2	0.005	0.015	0.16	32	3
3	1	4	0.003	0.008	0.18	60	3
4	1	6	0.002	0.006	0.19	95	3
5	2	1	0.013	0.038	0.10	8	3
6	3	1	0.015	0.045	0.08	5	3
7	1	1	0.008	0.025	0.20	25	3
8	2	2	0.008	0.025	0.20	25	3
9	3	3	0.008	0.025	0.20	25	3
10	1	1	0.008	0.060	0.13	17	8
11	2	2	0.008	0.060	0.13	17	8
12	3	3	0.008	0.060	0.13	17	8

3.4.4 SERS Efficiency of np-AgMSs

To use np-AgMSs as SERS substrates, the SERS property of the obtained np-AgMSs was investigated using *p*-aminothiophenol (PATP) as a Raman probe. Solution of 5 µL, 10^{-6} M PATP was pipetted into the microfluidic device containing np-AgMSs. The incubation time between PATP and np-AgMSs was studied in the range of 0-30 min. Then, the np-AgMSs were washed using 1 mL of absolute ethanol by pipetting the solution into the microchannel. Then, the device containing np-AgMSs was dried in an oven at 55 ºC for 1 h. SERS spectra were collected using a DXR Raman microscope. Laser power of 1 mW of a 532 nm excitation wavelength with 3.1 µm in diameter laser spot size was used as an incident light. All experiments were performed using a 50x objective lens. The laser beam was focused onto the center of a np-AgMS particle, as shown in **Fig 3.6 (c)**. SERS spectra were collected using an exposure time of 2 s with 16 accumulations. All SERS spectra were used without any spectral correction and each SERS spectrum represented each SERS substrate particle. All SERS spectra presented herein were averaged from 30 SERS spectra of 30 np-AgMSs particles.

3.4.5 Determination of SCN^- in Saliva

The np-AgMSs obtained from on-chip synthesis were used as SERS substrates for determination of SCN^- in saliva. Artificial saliva was used as a matrix blank for validation of the method. SCN^- solution was prepared in the concentration range of 1-50 µM in Milli Q water. A calibration curve was plotted between concentration of SCN^- and SERS intensity at a wavenumber of 2,117 cm^{-1}. To construct a calibration curve, 5 µL of each SCN^- solution was pipetted into the microfluidic device containing tetrapod np-AgMSs. In order to maximize the sensitivity, incubation time between SCN^- and np-AgMSs was studied in the range of 1-40 min. After the incubation step, 1 mL of air was pipetted into the microchannel to remove all solutions. Then, Raman spectra were collected and the intensity at a wavenumber of 2,117 cm^{-1} was used for data processing. To increase the sensitivity of the detection, the power of laser was increased from 1 to 10 mW. Limit of detection (LOD) and limit of quantitation (LOQ) were calculated using 3 and 10 signal to noise ratios, respectively. Intraday and interday precisions were also studied by spiking 3 concentrations of SCN^-, including 4, 8 and 12

mM, into artificial saliva. The spiked solutions were diluted 1,000 times before being used to perform the quantitative detection of SCN^-. For intraday precision, the experiment from the spiking step to the detection was repeated for 10 times in the same day. For interday precision, the same experiment was repeated for 3 times for each 3 consecutive days. Then, percent relative standard deviation (%RSD) of SERS signals obtained from each experiment was calculated using Equation 3.2 to determine the precisions;

$$\%RSD = \frac{SD}{\bar{x}} x100 \qquad (3.2)$$

where SD is standard deviation and $\bar{x}$ is averaged SERS intensity at a wavenumber of 2,117 cm^{-1}.

Accuracy of the method for determination of SCN^- in saliva was also investigated using the spiking technique. SCN^- standard solutions at 4, 8 and 12 mM were spiked into artificial saliva. Then, the solutions were diluted 1,000 folds to have the concentrations in the linear rage of the calibration curve. Recovery percentage of the spiked SCN^- was calculated using the Equation 3.3;

$$\%Recovery = \frac{SERS\ signal_{\ Spiked\ sample} - SERS\ signal_{Sample}}{SERS\ signal_{SCN^-\ standard}} x100 \qquad (3.3)$$

CHAPTER IV
RESULTS AND DISSCUSION

4.1 Part I Determination of GSH in Pharmaceutical Product

The determination of GSH using the reversed reporting technique which was purpose by Ozaki and co-workers [30]. The idea of the technique was to detect the decreasing of SERS signal after the replacement of a reporting agent with GSH. GSH is a large organic molecule comprising of three amino acids, including glutamic acid, L-cysteine and L-glycine [29]. GSH is a polar molecule without c-c stretching and also classified as a non-polarized or Raman inactive molecule. The overall procedure of the reversed reporting technique is shown in **Fig. 4.1**.

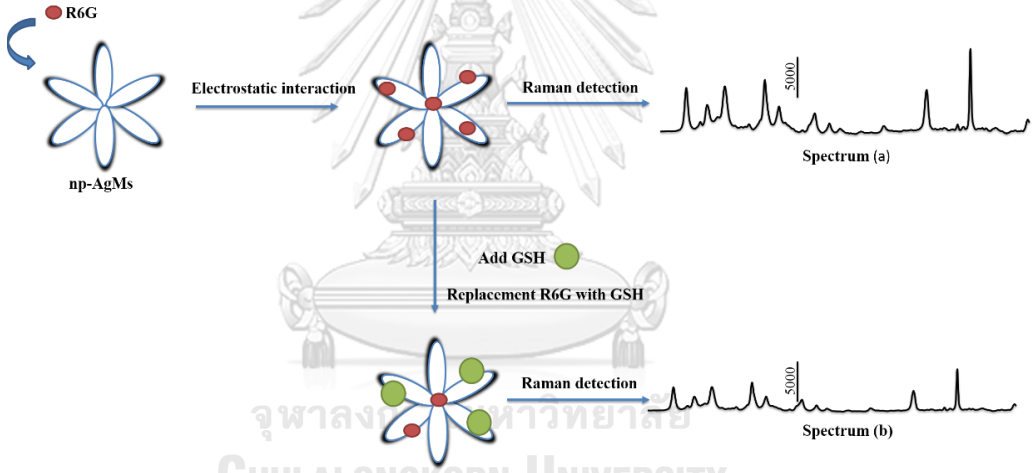

Figure 4.1 An indirect detection mechanism of GSH using a reversed reporting technique. R6G was attached to np-AgMSs via electrostatic interaction. The SERS signal of R6G-np-AgMSs was collected. Then, R6G molecules on np-AgMSs were replaced with GSH to form np-AgMSs-GSH. SERS signal of the remaining R6G-np-AgMSs was collected

4.1.1 Characterization of np-AgMSs

The np-AgMSs were obtained from Cl^- induced precipitation of $Ag(NH_3)_2^+$ followed by galvanic replacement of AgCl using an Zn plate as a sacrificed metal. The np-AgMSs were characterized using SEM. Results from SEM/EDS showed that the

particles were 100% Ag^0 without Cl^-. The structure of np-AgMSs was porous hexapod with the pore size in the range of 60-65 nm which was in the range of surface plasmon resonance (SPR) active [20]. Since the pores covered all over the particle surface, the particles were called porous like or mesoporous materials [68]. The particle size was approximately 20 μm which was easily observed under a Raman microscope [68]. An SEM image of np-AgMSs is shown in **Fig. 3.1(c)**.

4.1.2 Effect of Flow Rate on the Embedded np-AgMSs

The np-AgMSs which were embedded in the microchannel were only drop-casted using a micropipette. The embedded np-AgMs interacted with the silanol group of the PDMS channel via electrostatic interaction [72]. To obtain reproducible results, it was necessary to test the sticking ability of the particles on the surface of PDMS. To do that, Milli Q water was pumped through the microchannel. To find the maximum flow rate that could be used in the experiment without losing significant amount of np-AgMSs particles, different flow rates varied from 0 to 30 μL min^{-1} (flow velocities of 0-16.68 cm^3 s^{-1}) were studied. Subsequently, images of np-AgMSs in the microchannel were taken using an inverted optical microscope with a 10x objective lens. Results showed in **Fig. 4.2**. The flow rate that can be used to retain the embedded np-AgMSs was 15 μL min^{-1}. However, using the flow rate at 15 μL min^{-1} could cause the leakage of solution in the long run due to too high pressure. To ensure that there was no particle loss and no leakage, a flow rate of 10 μL min^{-1} was chosen as a suitable flow rate for all experiments.

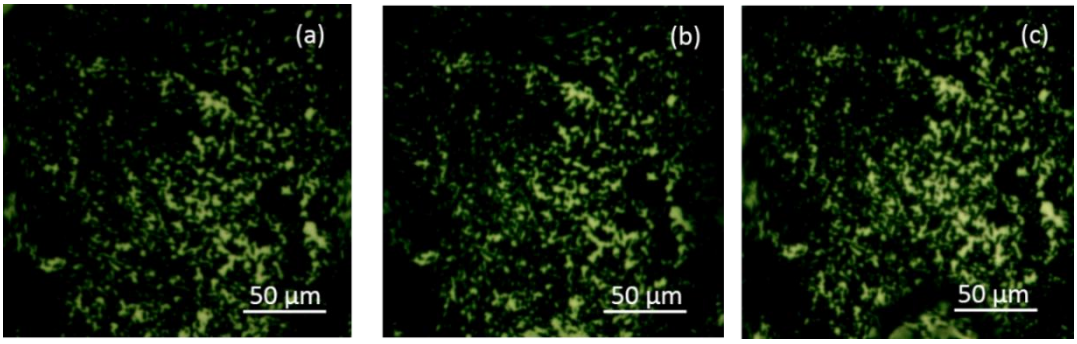

Figure 4.2 Images of the embedded np-AgMs after pumping milli Q water through the microchannel using different flow rates of (a) 0, (b) 15 and (c) 30 μL min^{-1}.

4.1.3 On-Chip SERS Detection

In general, SERS substrates should not provide SERS signal. To confirm that, an SERS spectrum of pure np-AgMSs was measured. Results showed a flat base line without any peak, as shown in **Fig 4.3(a)**, which indicated that the surface of SERS substrate was clean without any SERS active molecule. The next step was to measure SERS signal from R6G which was a Raman reporter in the reversed reporting technique. R6G is well known as a strong fluorescence dye [73] which also provided high polarization from the conjugated double bonds in its structure [31]. Although R6G bonded with np-AgMSs caused fluorescence quenching, high concentrations of R6G could cause fluorescence signal. Sensitivity of the technique would be decreased due to the broad fluorescence peak of R6G at 542 nm [74].

To avoid the fluorescence problem, a suitable concentration of R6G was studied. Results showed that 10^{-5} M R6G was the maximum concentration that could be used to provide the highest SERS signal without the interference from fluorescence. An SERS spectrum of R6G is shown in **Fig. 4.3(d)**. So, R6G at a concentration of 10^{-5} M was chosen as a Raman reporter. Electrostatic interaction between R6G and np-AgMSs could form between the positive charge of R6G and the negative charge of np-AgMSs [34, 75]. The reaction time between R6G and np-AgMSs was studied to maximize the SERS signal. The experiment was performed by pumping 10^{-5} M R6G into the microchannel at a flow rate of 10 μL min^{-1} for 1 min. The reaction time between 15-90 min was studied. SERS spectra of R6G-np-AgMs were collected using a 532 nm laser as an incident light. The obtained SERS spectra are shown in **Fig. 4.3(d)**. Peaks at wavenumbers of 1,311, 1,365, 1,512, 1,575 and 1,653 cm^{-1} are assigned to an aromatic c-c stretching vibration. Another band at 1,182 cm^{-1} corresponded to aromatic C-H bending of R6G [36, 62]. In order to obtain the highest sensitivity, the peak at a wavenumber of 1,365 cm^{-1}, which was the highest SERS signal without the fluorescent effect, was chosen as a representative SERS signal for further investigation**.** Results from the incubation time (between R6G and np-AgMSs) study showed that SERS signal increased when increasing the incubation time from 45 to 60 min. However. SERS signals were constant after 60 min, as shown in **Fig. 4.4**. Therefore, the optimized

incubation time between R6G and np-AgMSs to obtain the highest SERS signal was found to be 1 h.

4.1.3.1 SERS Detection of GSH

GSH exhibits relatively low Raman signal even in a solid state, as shown in **Fig. 4.3(b)**. Moreover, using np-AgMSs as SERS substrates could not enhance Raman signal of GSH, as shown in **Fig. 4.3(c)**. By using reversed reporting technique which used R6G as a Raman reporter, R6G capped onto the surface of np-AgMSs with electrostatic interaction provided high-SERS signal. However, SERS signal was decreased in the presence of GSH molecules. GSH having thiol group interacted with np-AgMSs with a stronger interaction than the interaction between R6G and np-AgMSs. Therefore, R6G was replaced with a GSH molecule to form a GSH-np-AgMs complex which was Raman inactive. Consequently, SERS signal was decreased relatively to the increase in GSH concentration. The decrease in SERS signal after the replacement of R6G by GSH is shown in **Fig. 4.3(e)**. To obtain the highest sensitivity for the detection of GSH, the incubation time between GSH and R6g-np-AgMS was studied in the range of 1-20 min. Results showed that SERS signal was decreased when increasing the reaction time from 1-10 min. After 10 min, SERS signal was constant, as shown in **Fig. 4.4**. Therefore, 10 min reaction time between GSH and R6G-np-AgMs was chosen.

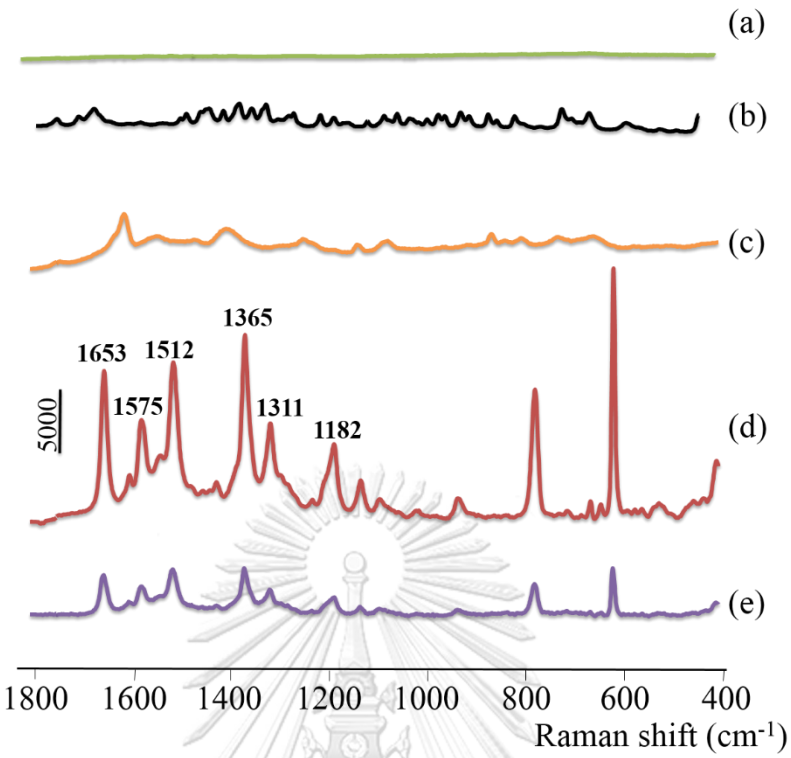

Figure 4.3 Raman spectra of (a) np-AgMSs, (b) solid GSH, (c) np-AgMSs with GSH, (d) np-AgMSs with R6G and (e) np-AgMSs with R6G in the presence of 10^{-3} M GSH.

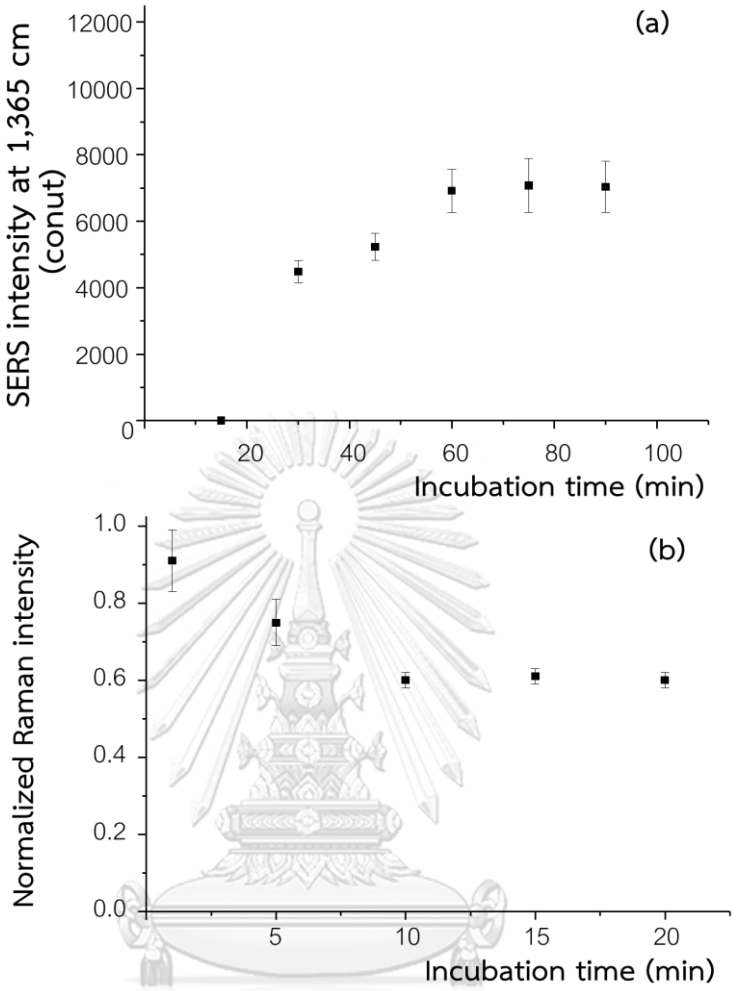

Figure 4.4 Optimization of incubation times for (a) 10^{-5} M R6G with np-AgMSs and (b) 10^{-5} M GSH with R6G-np-AgMSs.

4.1.3.2 Quantitative Detection of GSH

The decrease in SERS signal was strongly related to the amount of GSH in the solution. A calibration curve was plotted between the logarithm of GSH concentration and the normalized SERS signal.

To construct a calibration curve, various concentrations of GSH in the range of 10^{-8}-10^{-3} M were prepared and measured for SERS signal. Results showed that the replacement of R6G with GSH causing the decrease in SERS signal which was easily observed at the wavenumber of 1,365 cm^{-1}, as shown in **Fig. 4.5**. Moreover, the

decrease in SERS signal corresponded to the amount of GSH in the sample. The calibration curve is shown in **Fig. 4.6**. A linear range was found to be in the range of 10^{-8}-10^{-3} M with a correlation coefficient (R^2) of 0.9760. The lowest concentration of the calibration curve was found to be 10^{-8} M.

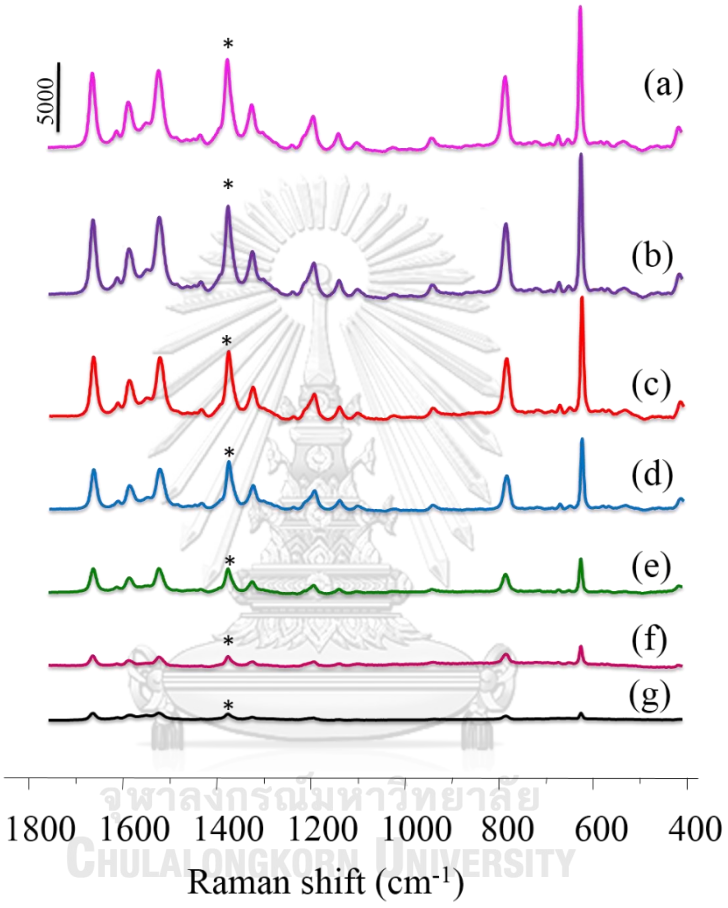

Figure 4.5 SERS spectra of 10^{-6} M R6G (a) with the presence of GSH in the concentration range of 10^{-8}-10^{-3} M (b-g). An SERS marker band for further quantitative analysis of GSH was at 1,365 cm^{-1}.

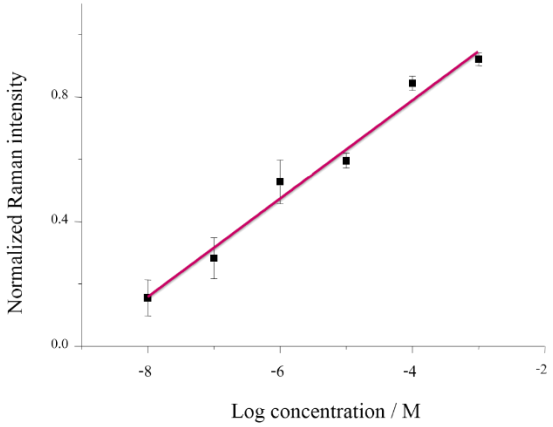

Figure 4.6 A calibration curve of glutathione in the concentration range of 10^{-3}-10^{-8} M with R^2 = 0.9760.

4.1.4 Reusability of np-AgMSs

The microfluidic device with embedded np-AgMSs allowed the solution flow through several times without damaging the particles. To reuse the np-AgMSs, the surface of the particles was clean up using a strong reducing agent. The process was also called chemical regeneration. In this work, $NaBH_4$ was chosen as a reducing agent to clean the particle surface. After the measurement of GSH, 1 mL of 1 M $NaBH_4$ was pumped into the microchannel at a flow rate of 10 µL min^{-1}, followed with Milli Q water to clean $NaBH_4$ and organic residues from the particle surface. After the cleansing step, SERS signal of the re-used np-AgMSs was recorded. Results showed a flat baseline with no SERS signal, which indicated that the surface of np-AgMSs was clean, as shown in **Fig. 4.7 (cycle 1)**, and was be able to reuse. Then the cleaned np-AgMSs were re-used to perform the experiment all over again for two more cycles. Results showed good reproducibility of SERS signal after the particles being reused for 3 times. The results indicated that the np-AgMSs could be regenerated up to 3 cycles of experiment without significant change of SERS signal. According to the reusability of the np-AgMSs, the same microfluidic device could be used several times without preparing new devices which provided advantages of cost-saving and reduction in waste and time.

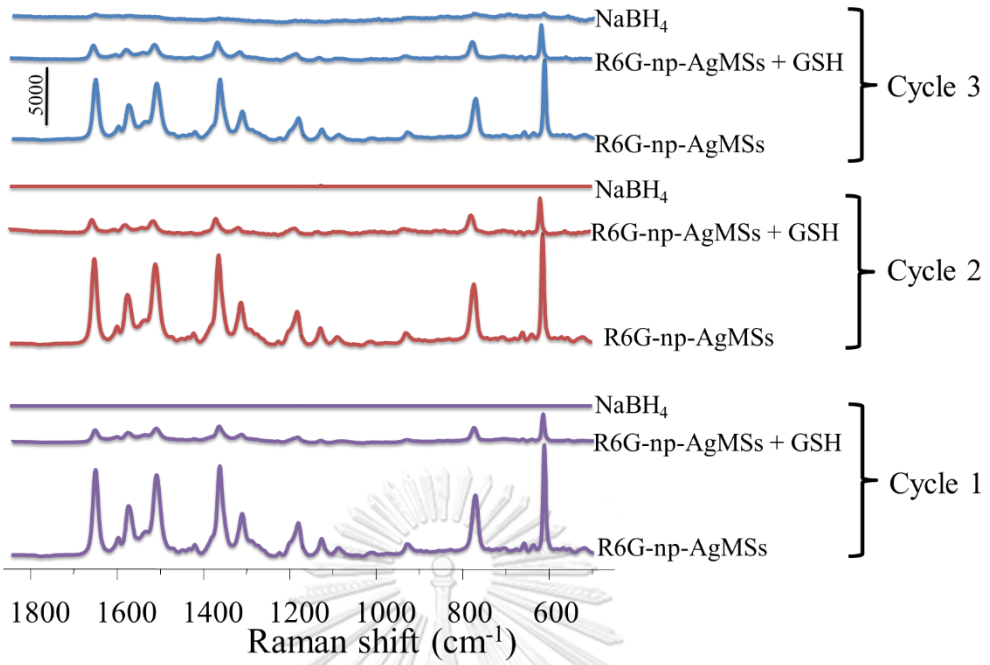

Figure 4.7 Raman spectra of R6G-np-AgMs, R6G-np-AgMs in the presence of 10^{-5} M GSH and $NaBH_4$ before (cycle 1) and after the regeneration process (cycles 2 and 3) using $NaBH_4$.

4.2 Part II Synthesis of np-AgMSs using microfluidic system

4.2.1 On-chip Synthesis of AgCl Sacrificial Templates

The synthesis of np-AgMSs in this work used Cl^- induced precipitation of $Ag(NH_3)_2^+$ to create AgCl templates [55]. Then, the AgCl precipitates were chemically reduced using a reducing agent to form np-AgMSs. This method is considered as a template method. The synthesis of AgCl templates started with the formation of a $Ag(NH_3)_2^+$ complex. The solution of 1 mL, 0.05 M $AgNO_3$ and 1 ml, 0.15 M NH_4OH were pre-mixed off-chip. NH_4OH was used as a shape controlling agent. The concentration of NH_4OH was used in excess compared to the concentration of $AgNO_3$ in order to make sure that there was excess NH_4OH left in the solution. Regarding to high complex formation constant (K_f) of Ag^+ and NH_3, complexation between Ag^+ and NH_3 could occur easily, as shown in **Equation 4.1** [55].

$$Ag^{+}_{(aq)} + 2NH_{3\,(aq)} \rightleftharpoons [Ag(NH_3)_2]^{+}_{(aq)};\ K_f = 1.6 \times 10^{7} \quad (4.1)$$

$$AgCl_{(s)} \rightleftharpoons Ag^{+}_{(aq)} + Cl^{-}_{(aq)};\ K_{sp} = 1.77 \times 10^{-10} \quad (4.2)$$

$$AgCl_{(s)} + 2NH_{3\,(aq)} \rightleftharpoons [Ag(NH_3)_2]^{+}_{(aq)} + Cl^{-}_{(aq)};\ K = K_f \times K_{sp} = 2.83\times10^{-3} \quad (4.3)$$

A flow-focusing microfluidic device composed of 3 inlets for fluidic access and 1 outlet was chosen for the synthesis of np-AgMSs. Flow-focusing configuration composed of two side flows and one central flow. This design could reduce the diffusion distance between two reactants from the side flows and central flow, causing rapid mixing within a microfluidic channel [76].

The $Ag(NH_3)_2^{+}$ complex solution was loaded into 1 ml syringe and pumped into the middle inlet of the flow-focusing microchannel. The other reactant which was 0.2 M NaCl was loaded into 2 sets of 1 mL syringes and pumped into the side inlets of the microchannel. The Cl^{-} and $Ag(NH_3)_2^{+}$ solutions were rapidly mixed and AgCl was generated simultaneously in the middle of microchannel. The size of the precipitated AgCl was big enough to be easily observed under a normal microscope, as shown in **Fig. 4.8(b)**. Although AgCl is sparingly soluble in water (K_{sp} = 1.77 × 10^{-10}), as shown in **Equation 4.2**, in NH_4OH solution it can form water soluble $[Ag(NH_3)_2]^{+}\ Cl^{-}_{(aq)}$ complex [77], as shown in **Equation 4.3**. Therefore, to induce precipitation of AgCl, relatively high concentration of Cl^{-} was required.

Due to hydrophobic property of unmodified PDMS surface, surface fouling of molecules could be observed on PDMS surface [78]. According to this phenomenon, AgCl seeds, which are hydrophobic, were found to adsorb on the PDMS surface. Consequently, the nucleations were developed into seeds and grew into larger AgCl particles. The seeds grew into bigger particles which were easily to be observed under a microscope. The growth mechanism followed the LaMer's model [79]. SEM was used to get more details of the AgCl particles. Results showed the symmetrical growth of the particles, which suggested that the particles grew via the atom mediated growth pathway in which free atoms in the solution diffused to accumulate onto the specific area of the seed surface [50, 79].

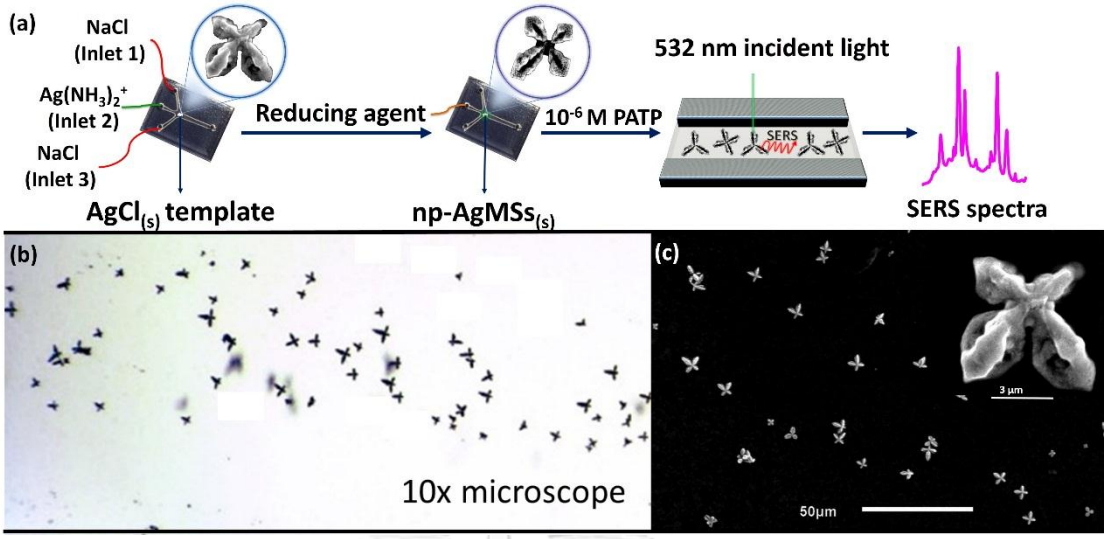

Figure 4.8 a) Experimental steps of the synthesis of np-AgMSs. On-chip synthesis was performed using a flow-focusing microfluidic device composing of 3 inlets and 1 outlet (the channel dimensions were 300 µm wide and 100 µm deep). Images of AgCl microstructures synthesized within a microchannel were taken using (b) a microscope (c) SEM.

4.2.2 Effect of Reactant Concentration on the Morphology of AgCl Microstructures

Effects of reactant concentration on the structure of AgCl templates were previously reported by Gatemala and coworkers [47]. In high Cl^- conditions, an AgCl octapod family was observed. On the other hand, in high NH_4OH conditions, an AgCl hexapod family was observed. To study the effect of concentration in batch systems, new solutions have to be prepared either by diluting from stock solutions or freshly preparing. However, microfluidic systems offer a better way of changing reactant concentration by adjusting the flow rate of reactant itself. For a flow-focusing design, if the central flow rate is fixed and the flow rates of side inlets are equally increased, it can be assumed that the final concentration of the side flow reactant is increased proportionally to the increased flow rate. To study effects of reactant concentration, the experiments were divided into two groups for Cl^- rich and NH_4OH rich environments.

4.2.2.1 Cl^- Rich Environment.

The first group of experiment was to investigate the effect of Cl^- concentration on the structure of AgCl templates. The ratios of $[Cl^-]/[Ag^+]$ and $[NH_4OH]/[Ag^+]$ represented the amounts of Cl^- and NH_4OH in the system, respectively. The concentration ratio was taken into account to study the effect of reactant concentration because in every experiment, the total flow rate was altered when fixing the flow rate of one reactant and changing the other. The flow rate of $Ag(NH_3)_2^+$ was fixed constant and the flow rates of Cl^- were changed from 1 to 6 μL min^{-1}, as shown in **Table 4.1(Exp. 1-4)**. This resulted in the ratio of $[Cl^-]/[Ag^+]$ being increased from 16 to 32, 60 and 95 and the ratio of $[NH_4OH]/[Ag^+]$ was kept constant at 3. Results obtained from the study of effect of Cl^- were shown in **Fig 4.9**. The structure of AgCl obtained from the low $[Cl^-]/[Ag^+]$ ratio of 16 was found to be cubic. When increasing the $[Cl^-]/[Ag^+]$ ratio to 32, 60 and 95, respectively, it was found that the AgCl structure was developed from cubic structure into tetrapods at high $[Cl^-]/[Ag^+]$ ratios or high Cl^- environment.

To preserve the lowest total energy of the system, AgCl generally crystallizes into a cubic structure under thermodynamic control [50]. The crystal is enveloped by the lowest surface energy of {100} facets [47, 49, 80]. The growth on the corners of cubic seeds {111} and tetrahedron seeds {100} are preferable compared to the edge and face [48, 49]. However, as mentioned above that the AgCl seeds were adsorbed onto the PDMS surface, leading to the structure growth into 2-dimensional structure instead of 3-dimentional structure which normally occurs in typical batch synthesis [47]. Therefore, in Cl^- rich environment, the cubic seeds grew via {111} faster than {100} and {110} [47]. Consequently, the cubic seeds grew into tetrapods. The growth mechanisms are shown in **Fig. 4.10(a)**.

4.2.2.2 NH_4OH Rich Environment.

The second group of experiments was to investigate the effect of $Ag(NH_3)_2^+$ on the structure of AgCl templates, the side flow was fixed and the central flows were varied from 1 to 3 μL min^{-1}, as shown in **Table 4.1(Exp. 1, 5-6)**. In terms

of concentration ratio, the ratio of $[NH_4OH]/[Ag^+]$ was constant at 3 and the ratio of $[Cl^-]/[Ag^+]$ was decreased from 16 to 8 and 5, respectively. Results showed that when decreasing the $[Cl^-]/[Ag^+]$ ratio, the AgCl structure was changed from cubic structure to tetrahedron, as shown in **Fig. 4.9 (Exp. (1) to (5))** and was further developed into tripod, as shown in **Fig. 4.9 (Exp. (5-6))**.

In NH_4OH rich environment (Exp. (5-6)), it was previously reported that selective etching occurred on the {111} corners of cubic structure. Consequently, the corners of cubic seeds were dissolved at a higher rate compared to {110} and {100} [47]. This phenomena could lead to the structural change of AgCl templates from cubic in Cl^- rich environment to tetrahedron in NH_4OH rich environment. Moreover, the tetrahedral seeds were grown faster in {100} than {110} and {111} [47]. Consequently, the tetrahedral seeds were grown into tripods. The growth mechanisms are shown in **Fig. 4.10(b)**.

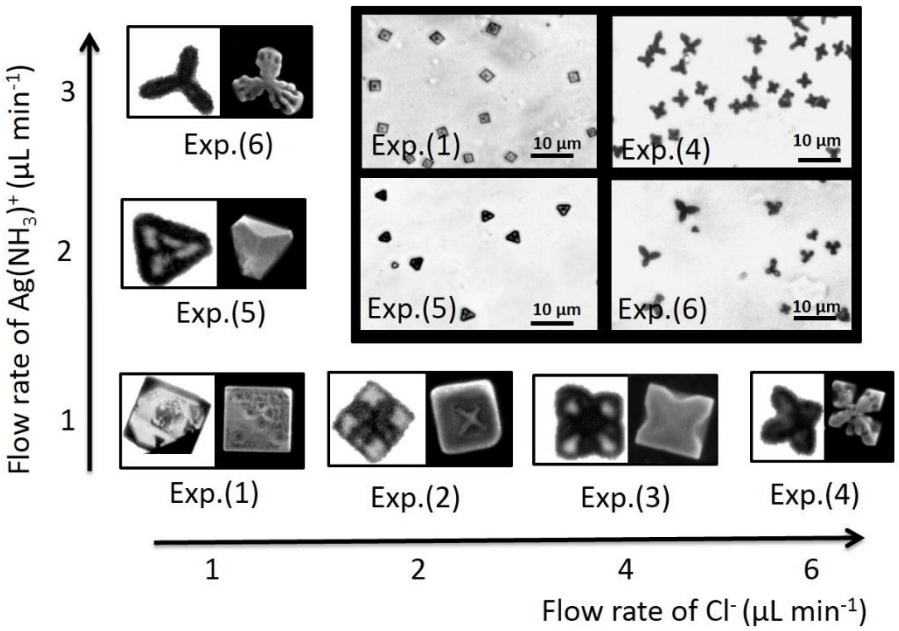

Figure 4.9 Microscope and SEM images of AgCl structures transforming from cubic (Exp. (1)) to tetrapod (Exp. (4)) when increasing the flow rate of Cl^- and from tetrahedron (Exp. (5)) to tripod (Exp. (6)) when increasing the flow rate of $Ag(NH_3)_2^+$.

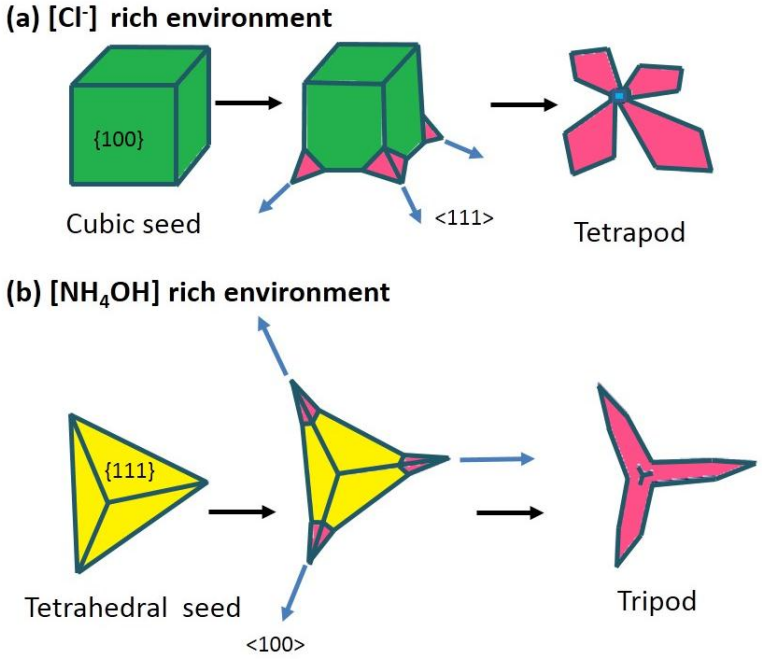

Figure 4.10 The proposed AgCl growth mechanisms in (a) Cl^- rich and (b) NH_4OH rich environments, respectively.

4.2.3 Effect of Flow Velocity on the Structure of AgCl

To study the effect of flow velocity, the concentration of all reactants were kept constant. The experiments were divided into two parts in order to study effect of flow velocity under both high Cl^- and high NH_4OH environments. To ensure that the experiments were in Cl^--rich and NH_4OH-rich environments, the ininital concentrations of Cl^- and NH_4OH were increased to 0.2 M and 0.060 M, respectively. The flow ratio of the side flow and central flow was kept constant at 2:1 to maintain the concentration of both reactants. Total flow rate was increased from 3 to 6 and 9 μL min^{-1} which were equal to flow velocities of 0.17, 0.33 and 0.50 cm s^{-1}, respectively. All experimental conditions are shown in **Table 4.1 (Exp. (7-9)** and **Exp. (10-12)** for high Cl^- and high NH_4OH environments, respectively.

Results showed that for high Cl^- environment, AgCl tetrapods were observed, as described above. On the other hand, for high NH_4OH environment, AgCl tripods were observed. For high Cl^- environment, when increasing the total flow velocity from 0.17 to 0.33 and 0.50 cm s^{-1}, the averaged AgCl particle size was decreased from 6 to 4 and 2 μm respectively, as shown in **Fig. 4.11 (Exp. (7-9))**. Similar results of the relation

between flow velocity and the obtained particle size could be observed for high NH_4OH environment, as shown in **Fig. 4.11 Exp. (10-12)**.

As mentioned that the growth mechanism of AgCl in this work was the atom mediated growth [50, 79]. Free atoms in the solution diffused into specific location on the AgCl seeds and grew into bigger particles. Accordingly, at high flow velocities, the neucleation of AgCl occurred at a higher rate compared to low flow velocities [81]. Therefore, at high flow velocities, AgCl particles grew rapidly into smaller particles compared to the particles obtained at low flow velocities. The experimental results were in good agreement with the LaMer's model [82]. Moreover, this phenomena could lead to an alternative approach to control particle size for the synthesis without preparing new reagents. By increasing the total flow velocity, a smaller particle size could be obtained. In vise versa, by decreasing the total flow velocity, a bigger particle size could be obtained.

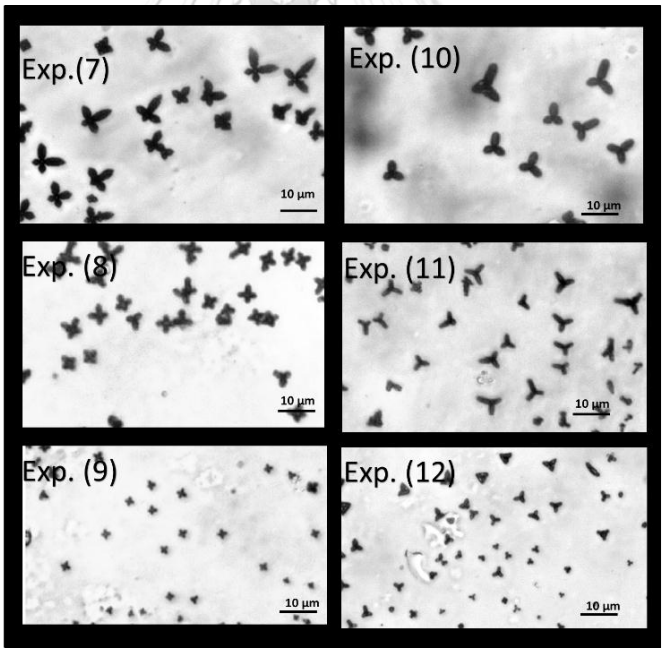

Figure 4.11 Microscopic images of AgCl microstructures synthesized under different total flow velocities. The size of particles was found to be decreased from 6 to 4 and 2 µm (for Exp. (7)-(9) and Exp. (10)-(12)) when increasing the total flow velocity from 0.17, 0.33 and 0.50 cm s^{-1}, respectively. The AgCl microstructures were synthesized under Cl^--rich environment (Exp. (7)-(9)) and NH_4OH-rich environment (Exp. (10)-(12)), respectively.

Table 4.1 Experimental conditions for the synthesis of AgCl microstructures.

Exp.	Flow rate (μL min^{-1})		Final concentration (M)			Ratio	
	central flow $[Ag(NH_3)_2]^+$	side flow Cl^-	Ag^+	NH_4OH	Cl^-	$\frac{[Cl^-]}{[Ag^+]}$	$\frac{[NH_4OH]}{[Ag^+]}$
1	1	1	0.008	0.025	0.13	16	3
2	1	2	0.005	0.015	0.16	32	3
3	1	4	0.003	0.008	0.18	60	3
4	1	6	0.002	0.006	0.19	95	3
5	2	1	0.013	0.038	0.10	8	3
6	3	1	0.015	0.045	0.08	5	3
7	1	1	0.008	0.025	0.20	25	3
8	2	2	0.008	0.025	0.20	25	3
9	3	3	0.008	0.025	0.20	25	3
10	1	1	0.008	0.060	0.13	17	8
11	2	2	0.008	0.060	0.13	17	8
12	3	3	0.008	0.060	0.13	17	8

4.2.4 On-chip Reduction of AgCl Templates.

After the fabrication of AgCl templates using Cl^- induced precipitation of $Ag(NH_3)_2^+$. When changing reagent concentration, four different structures of AgCl, including cubic, tetrahedron, tripod and tetrapod, were observed. The next step of the synthesis was chemical reduction of AgCl templates into zero-valent Ag^0. The key factor of this step was not only to create nanoporous of np-AgMSs but also to preserve the original AgCl structure. Although four different structures of AgCl templates were obtained, cubic was the simplest structure to observe the structural change in details. Therefore, cubic was chosen as a representative structure to observe the structural change which may have caused by the reducing agents. Three different reducing agents were chosen, including hydrazine (E^0 = -0.230 V) [54], ascorbic acid (E^0 = -0.066V)[83] and $NaBH_4$. (E^0 = -0.481 V) [54]. All three reducing agents have lower reduction potential (E^0) compared to E^0 of $Ag^+ \longrightarrow Ag^0$ in water (E^0 = +0.79 V) [54]. Therefore, chemical reduction of Ag^+ into Ag^0 occurred simultaneously with $\Delta G^0 < 0$ and $\Delta E^0 > 0$ [84]. For hydrazine, which is in a gas phase, was considered as the slowest reducing agent compared to the other two reducing agents which are in solutions. Although hydrazine has the highest reduction potential, it took time to diffuse into the microchanel. On the other hand, ascorbic acid has a lower reduction potential compared to $NaBH_4$. Therefore, ascorbic acid was considered as a moderate reducing agent and $NaBH_4$ was considered as the fastest reducing agent among the three reducing agents.

Results from microscope and SEM images showed that when using hydrazine as a reducing agent, the final structure of np-AgMSs after being reduced with hydrazine (**Fig. 4.12(b)**) could not retain the structure of AgCl templates (**Fig. 4.12(a)**). Only aggregated particles were observed. According to slow reduction rate, there was enough time for the crystals to re-crystallize in order to reduce the total energy of the system, which resulted in aggregated particles [43, 55]. From the result, it was concluded that hydrazine could not be used as a reducing agent because the structure of mother template could not be retained. On the other hand, from microscope and SEM images showed that the structure of final products retained the cubic structure after AgCl particles being reduced by ascorbic acid and $NaBH_4$ as reducing agents (**Fig.**

4.12 (c-d)). When using ascorbic acid and $NaBH_4$, the reduction was fast and the particles did not have time to recrystallize [43, 55]. Therefore, the structure of the AgCl templates was retained after the reduction. The transformation from AgCl to Ag^0 was easily observed by the color change from white AgCl precipitate in **Fig. 4.12(a)** compared to the dark Ag^0 (**Fig. 4.12(c-d)**) under a normal microscope.

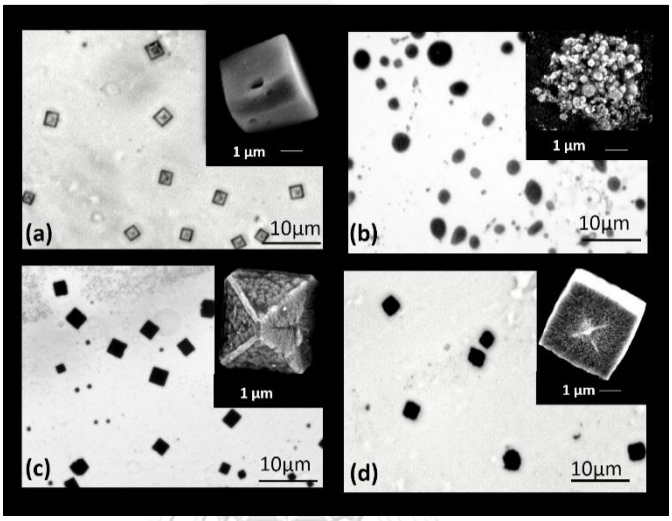

Figure 4.12 Microscope and SEM (the insets) images of AgCl microcrystals before reduction (a) and after reduction with (b) hydrazine, (c) ascorbic acid and (d) sodium borohydride, respectively.

To confirm that the product after being reduced with ascorbic acid and $NaBH_4$ was Ag^0, elemental analysis using SEM/EDS was performed. Results from SEM/EDS of AgCl templates before being reduced showed that the elemental composition of Ag:Cl was found to be 1:1 which confirmed that the component was 100% AgCl (**Fig. 4.13(a)**). After chemical reduction of AgCl templates, SEM/EDS showed that the percentage of Ag atoms was 99 % (**Fig. 4.13(b)**) which confirmed that the final products were np-AgMSs. Similar results from SEM/EDS were observed when using $NaBH_4$ as a reducing agent (**Fig.4.13(c)**).

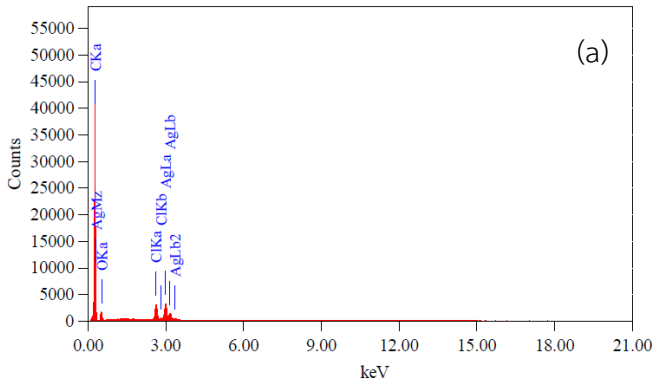

Thin Film Standardless Standard Quantitative Analysis
Fitting Coefficient : 0.3625

Element		(keV)	Mass%	Counts	Error%	Atom%	Compound	Mass%	Cation
C K	(Ref.)	0.277	79.98	258643.58	0.00	95.47			
O K		0.525	1.03	8575.50	0.16	0.92			
Cl K		2.621	4.02	30462.15	0.12	1.62			
Ag L		2.984	14.98	34108.33	0.11	1.99			
Total			100.00			100.00			

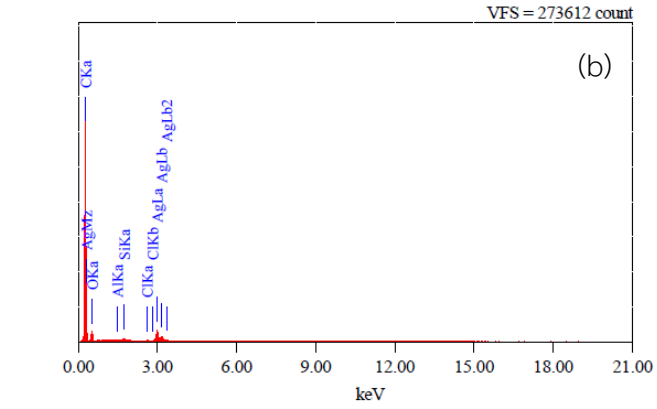

Thin Film Standardless Standard Quantitative Analysis
Fitting Coefficient : 0.3951

Element		(keV)	Mass%	Counts	Error%	Atom%	Compound	Mass%	Cation
C K	(Ref.)	0.277	87.48	1197802.75	0.00	97.37			
O K		0.525	1.30	46047.68	0.15	1.09			
Al K		1.486	0.03	1397.72	13.13	0.02			
Si K		1.739	0.39	17097.62	1.17	0.19			
Cl K		2.621	0.00	75.02	237.77	0.00			
Ag L		2.984	10.80	104121.74	0.18	1.34			
Total			100.00			100.00			

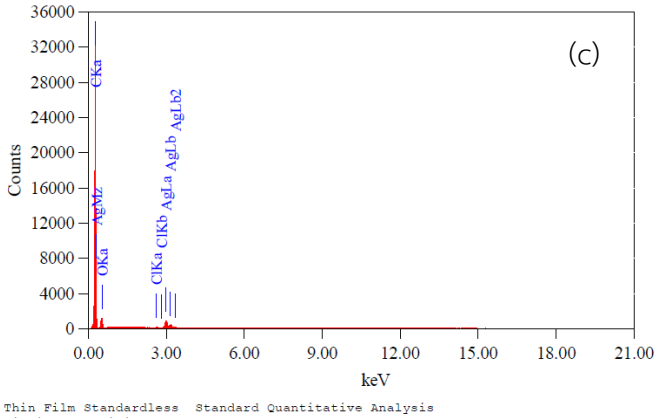

Thin Film Standardless Standard Quantitative Analysis
Fitting Coefficient : 0.4165

Element		(keV)	Mass%	Counts	Error%	Atom%	Compound	Mass%	Cation
C K	(Ref.)	0.277	93.39	205221.70	0.00	98.48			
O K		0.525	1.11	6283.30	0.18	0.88			
Cl K									
Ag L		2.984	5.50	8518.58	0.37	0.65			
Total			100.00			100.00			

Figure 4.13 Elemental mapping from SEM-EDS; (a) AgCl (b) AgCl reduced with $NaBH_4$ and (c) AgCl reduced with ascorbic acid.

The interconnected grain size of np-AgMSs obtained from ascorbic acid and $NaBH_4$ was approximately 80 nm and 100 nm, respectively. From the literature review, the smaller the interconnected grain size should provide the better SERS signal [40]. According to the results, the obtained np-AgMSs which was reduced with $NaBH_4$ should provide higher SERS signal due to smaller interconnected grain size compared to ascorbic acid. The distribution profiles of interconnected grain size of np-AgMSs are shown in **Fig. 4.14**

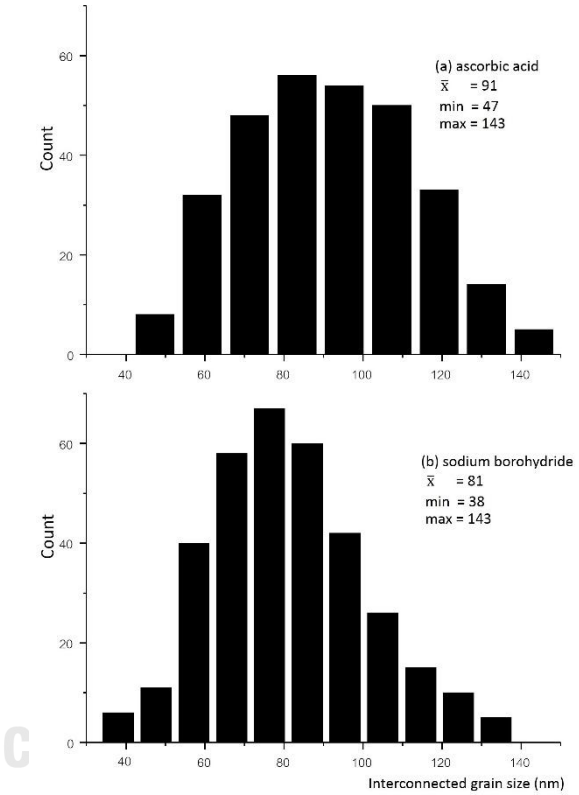

Figure 4.14 Interconnected grain size distribution of np-AgMSs obtained from using different reducing agents including; ascorbic acid and sodium borohydride.

4.2.5 SERS Property of np-AgMSs

The fabricated np-AgMSs were tested for SERS properties using 10^{-6} M PATP. SERS spectra obtained from np-AgMSs with different reducing agents were shown in **Fig. 4.15**. Results showed that when using AgCl as a substrate, there was no SERS signal of PATP because AgCl does not have surface plasmon property **Fig 4.12 (a)**. According

to aggregated Ag particles obtained from using hydrazine reducing agent, low SERS signal of PATP was observed (**Fig. 4.15(b)**). The interconnected grain size of np-AgMSs obtained from ascorbic acid and $NaBH_4$ reducing agents were in the ranges of 47-143 nm and 38-133 nm, respectively. According to the literature review, high sensitive SERS substrates should have the interconnected grain size in the range of 1-100 nm [20, 44]. The highest SERS signal was observed from np-AgMSs obtained from $NaBH_4$. Chemical reduction between np-AgMSs and $NaBH_4$ was occurred immediately, the np-AgMSs does not have enough time to rearrange or aggregate. Therefore, interconnected grain size obtained from using $NaBH_4$ as a reducing agent was smaller and narrower distribution, as shown in **Fig. 4.15**. Therefore, $NaBH_4$ was chosen as a reducing agent for further experiments.

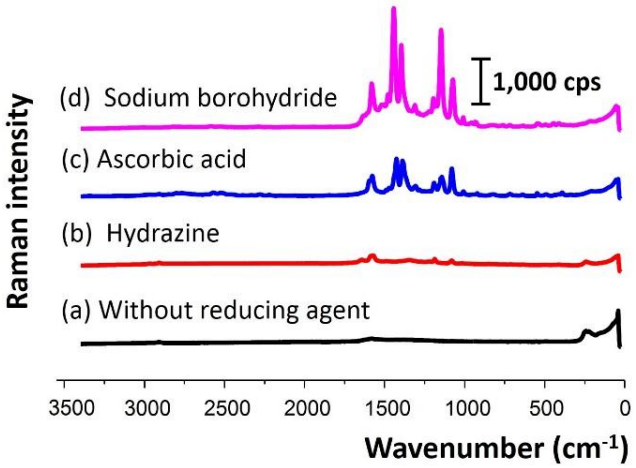

Figure 4.15 Raman spectra of PATP obtained when using the np-AgMSs as SERS substrates. The np-AgMSs were reduced by different reducing agents; (a) without a reducing agent, (b) hydrazine, (c) ascorbic acid and (d) sodium borohydride.

To study effect of the structure of np-AgMSs on SERS property, four different AgCl structures, including cubic, tetrahedron, tripod and tetrapod were reduced using $NaBH_4$. The obtained np-AgMSs with different structures (**Fig. 4.16**) were tested as SERS substrates for the determination of 10^{-6} M PATP. SERS spectra were collected and results showed that the multipod family (tripod and tetrapod) provided higher SERS signal than cubic and tetrahedron (**Fig. 4.17**). $NaBH_4$ was reduced from edge to center

of AgCl particle. The distance travel from edge to center of AgCl multipod structure were shorter compare to the cubic and tetrahedron. Therefore, cubic and tetrahedron took longer reduction time causing an aggregated on the center of the particle during the reduction. On the other hand, multipod family took shorter time to finish the reduction processed. Consequently, multipod family provided smaller interconnected grain size (40-65 nm, **Fig. 4.18(c-d)**) and narrower distribution compared to the cubic and tetrahedron (35-130 nm, **Fig. 4.18(a-b)**). Moreover, the multipod family also provided interconnected microparticles which could help improving the sensitivity of Raman signal [44]. According to SERS performance, both tripod and tetrapod provided high sensitivity. However, the tetrapod structure was prepared in a milder synthesis condition (low NH_4OH) compared to tripod which was synthesized in a high NH_4OH condition. Therefore, the tetrapod np-AgMSs were chosen as high sensitivity SERS substrates to demonstrate on-chip determination of SCN^- in saliva using SERS.

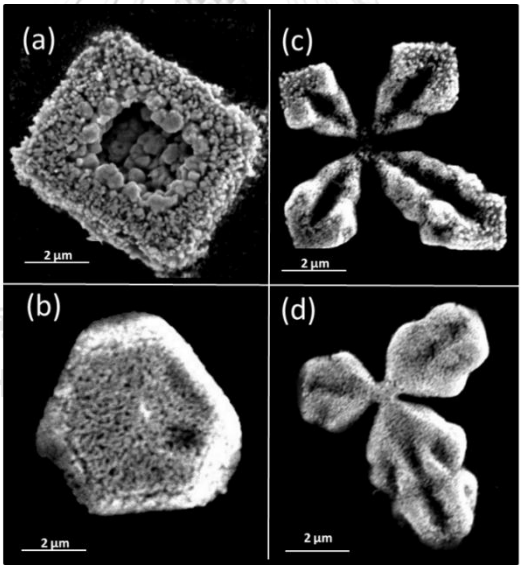

Figure 4.16 SEM images of np-AgMSs after being reduced by sodium borohydride; (a) cubic, (b) tetrahedron, (c) tetrapod and (d) tripod.

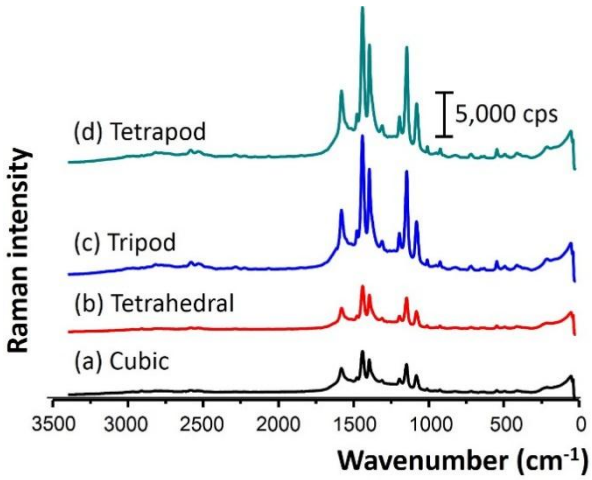

Figure 4.17 Raman spectra of PATP obtained from different structures of np-AgMSs; (a) cubic, (b) tetrahedron, (c) tripod and (d) tetrapod.

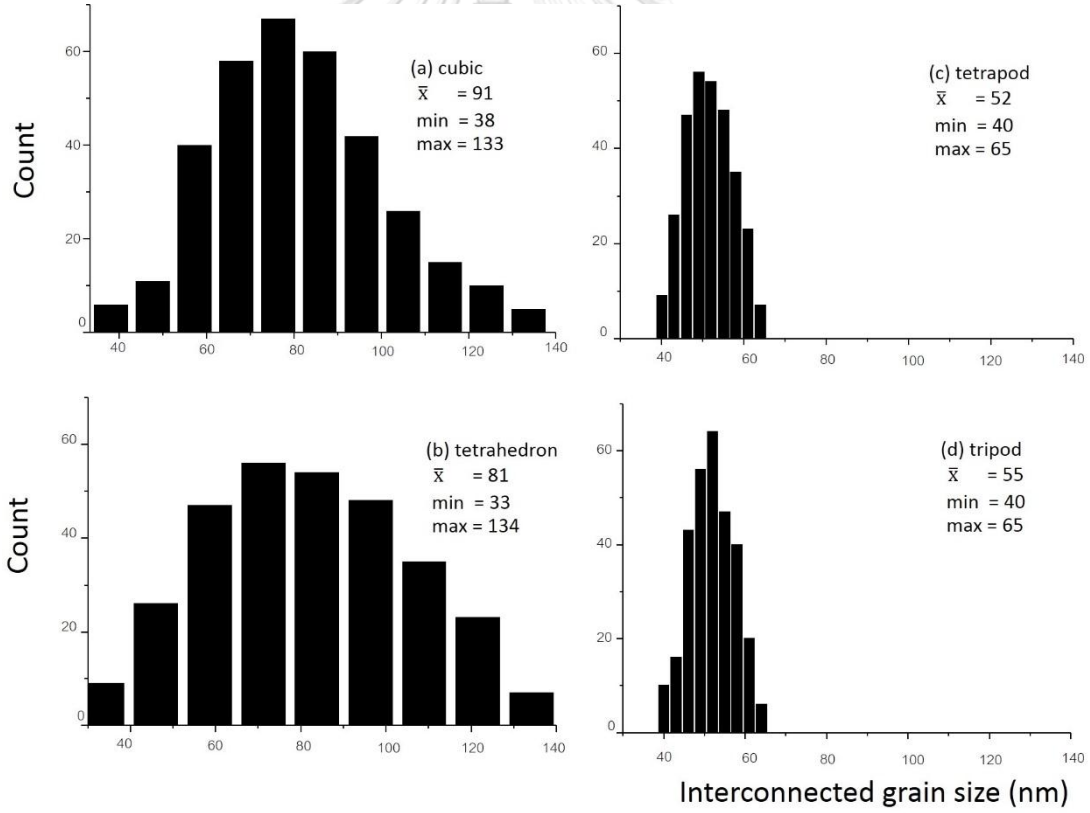

Figure 4.18 Interconnected grain size distribution of different np-AgMSs structures, including (a) cubic, (b) tetrahedron, (c) tetrapod and (d) tetrapod which were obtained from sodium borohydride as a reducing agent.

4.2.6 Quantitative Determination of SCN^- in Human Saliva

SCN^- is a toxic compound which is commonly found in saliva of smokers [65]. SCN^- is strongly bound to np-AgMSs surface through a sulfide bond (Ag-S) [85]. Raman technique not only provided high specificity through sulfide bond, but also provided fingerprinted spectra of -C≡N stretching mode of SCN^- at wavenumber 2,117 cm^{-1} [65]. Sample preparation process to separate analyte (SCN^-) from matrix (saliva) was not necessary due to the specificity of the technique which is mentioned above. To develop an analytical method for on-chip SERS substrate for the determination of SCN^- in saliva, the tetrapod np-AgMSs were chosen as SERS substrate. Tetrapod np-AgMSs were on-chip synthesized as described above. Reaction time between SCN^- and np-AgMSs in the microchannel was studied in the range of 0 to 40 min using SCN^- concentrations of 3, 10 and 18 µM. SERS signal at wavenumber of 2,117 cm^{-1} was collected. Results showed that SERS intensity was increased with the incubation time (**Fig. 4.19**) and the SERS intensity was constant after 30 min incubation time for all concentrations. Therefore, 30 min incubation was chosen.

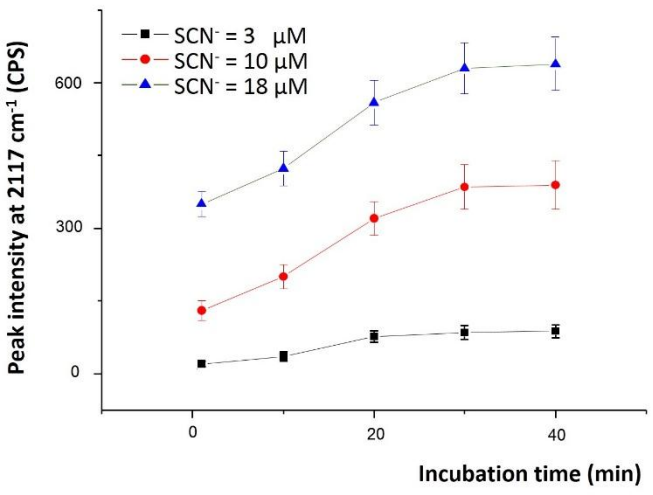

Figure 4.19 Effect of incubation time between SCN^- and np-AgMSs on SERS intensity at SCN^- concentrations of 3, 10 and 18 µM.

Analytical parameters, including a calibration curve, LOD and LOQ, were studied. A calibration curve was plotted to illustrate the relation between concentration of SCN^- and SERS intensity at the wavenumber of 2,117 cm^{-1}. The plot (Fig. 4.20) showed a good linear relation between concentration of SCN^- and SERS signal. A Linear range was found to be 1 to 20 µM. LOD and LOQ were calculated from 3 and 10 signal to noise ratios which were found to be 0.1 and 1.5 µM, respectively.

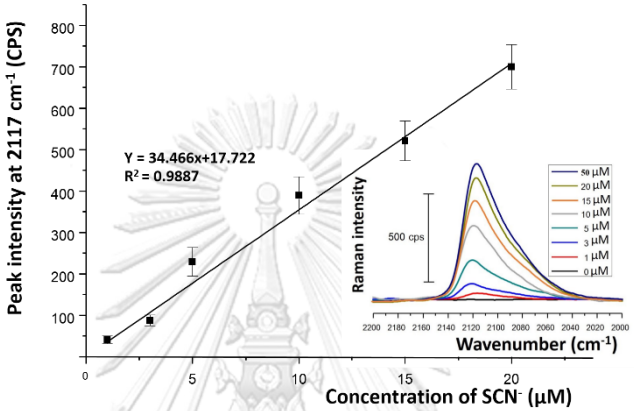

Figure 4.20 Linearity (1 to 20µM) of the on-chip SERS method for quantitative determination of SCN^- and the SERS spectra obtained from 1 to 50 µM SCN^- are shown in the inset.

Normally, the level of SCN^- in saliva found in non-smokers is in the range of 0.5 to 2 mM. [86] For smokers, the SCN^- concentration level in saliva is higher and can be up to 6 mM. [86] According to the linear range, saliva samples can be diluted up to 1,000 times. The dilution of sample not only reduced the viscosity of the sample but also minimized the interfering effect that could come up with sample matrix. Precision of the method in terms of reproducibility was also investigated. To study precision of the proposed method. The experiments were divided into two parts. For intraday precision, the experiments were performed using spiked technique. Standard SCN^- in the concentration of 4, 8 and 12 mM were added into artificial saliva. The detection of SCN^- were followed procedure in **section 3.4.5**. The experiments were duplicated 10 times within the same day. Results showed that the calculated RSD percentage (%RSD) of the SERS signal was found to be less than 9% which was acceptable according to

the association of official agricultural chemists (AOAC) standard [87] (**Fig. 4.21(a)**). For interday precision, the experiments were conducted 3 days and 3 duplicates for each day. Results showed that %RSD of SERS signal was found to be less than 6 % which is also acceptable according to the AOAC standard [87] (**Fig. 4.21(b)**).

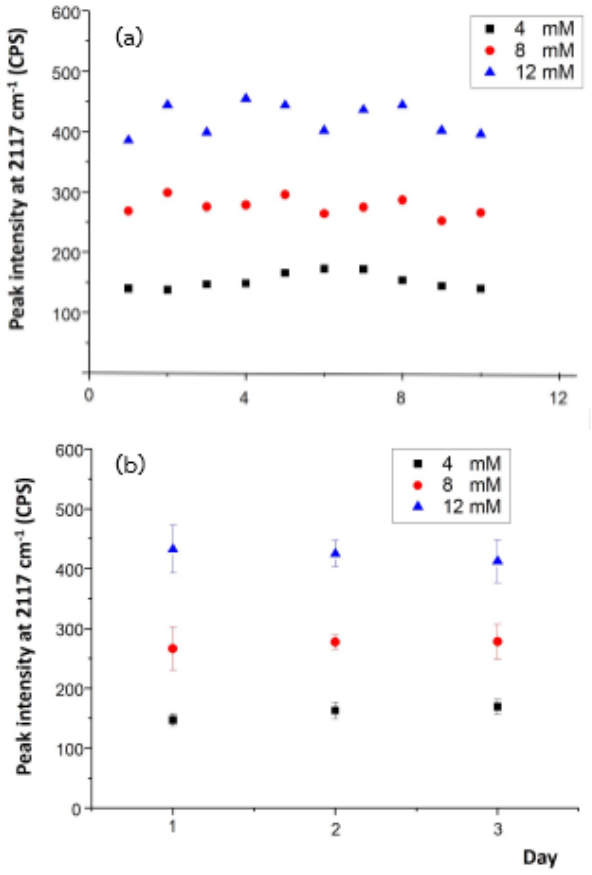

Figure 4.21 (a) intraday precision and (b) interday precision of SERS signal for the determination of SCN^- in artificial saliva.

In addition, accuracy of the proposed method was also investigated spiked matrix blank method was used. SCN^- at 3 different concentrations including 4, 8 and 12 μM, representing low, medium and high concentration, were used to study the accuracy. Standard solution of SCN^- concentration of 4, 8 and 12 mM were prepared in artificial saliva. The spiked samples were 1,000-fold diluted before SERS measurements. SERS signals were obtained and converted into concentrations using the equation from the calibration plot. Results showed that recovery–percentage

(%recovery) of all spiked SCN^- standards was found to be in the range of 90-110 %, as shown in Table 4.2. These indicated high accuracy and precision of the proposed method for the determination of SCN^- in saliva.

Table 4.2 Quantitative determination of SCN^- in artificial saliva.

Sample No.	SCN^- (mM)		%Recovery
	Added	Founded ± SD	
1	4	3.78 ± 0.32	94.50
	8	7.23 ± 1.03	90.38
	12	12.05 ±1.16	100.42
2	4	4.22 ± 0.39	105.50
	8	7.55 ± 0.33	94.38
	12	11.84 ± 0.63	98.67
3	4	4.41 ± 0.37	110.00
	8	7.57 ± 0.84	94.63
	12	11.46 ± 0.35	95.50

CHAPTER V
CONCLUSIONS AND FUTURE WORK

In this work, np-AgMSs were successfully used as on-chip SERS substrates. The np-AgMSs were both synthesized off-chip and on-chip. The synthesized particles were used as SERS substrates for the determination of SCN^- in artificial saliva and GSH using Raman spectroscopy.

For the determination of GSH, np-AgMSs were synthesized off-chip then embedded into the microfluidic channel. The reversed reporting method was used as an indirect approach for determination of GSH. R6G was used as a reversed reporting agent. SERS signal obtained from R6G-np-AgMs was proportionally decreased with the concentration of GSH. Analytical performance was studied and the results showed that Linear range was found to be 10^{-8}-10^{-3} M with R^2 = 0.9760. The lowest of calibration curve was found to be 10^{-8} M. Moreover, after the particles were washed with $NaBH_4$, it was found that the particles were reused up to 3 cycles without significant change in SERS signal.

For the determination of SCN-, np-AgMSs were synthesized on-chip using chloride induced precipitation of $Ag(NH_3)_2^+$. A flow-focusing microfluidic device was used as a microreactor for the synthesis. The synthesis started with off-chip preparing a complex of $Ag(NH_3)_2^+$. The solutions of $Ag(NH_3)_2^+$ and NaCl were then pumped into the microfluidic device for the synthesis. By systematically adjusting the flow rates of $Ag(NH_3)_2^+$ and NaCl, four different structures of AgCl were observed, including cubic, tetrahedron, tetrapod and tripod. After that, AgCl templates were reduced to form np-AgMSs. Three reducing agents including hydrazine, sodium borohydride and $NaBH_4$ representing as a slow, moderate and fast reducing agent, respectively were used. Results showed that when using $NaBH_4$ as a reducing agent, the narrowest distribution of interconnected particle grain size was obtained. Moreover, the structure of the mother AgCl template could be retained. The averaged particle size of the obtained np-AgMSs was in the range of 3-6 μM, which was easily focused under a microscope. Tetrapod np-AgMSs were chosen as SERS substrates for the determination of SCN^- in

artificial saliva because the structure provideed the highest SERS signal. The incubation time between SCN^- and the np-AgMSs in the microchannel was found to be 30 min. Linear range of the method for determination of SCN^- was in the range of 1-20 μM with R^2=0.9887. Calculated LOD and LOQ were found to be 0.1 and 1.5 μM, respectively. Accuracy in terms of %recovery of spiked SCN^- standard was found to be in the range of 90-110%. Reproducibility of SERS signal for the determination of SCN^- were achieved with %RSD less than 9% for both interday and intraday measurements.

Compared with batch synthesis, on-chip synthesis using a microfluidic system was found to be easy manipulation of the particle structure and also concentration of reactant only by adjusting the input flow rates. The device was low cost production. In addition, the microfluidic approach allowed high-throughput synthesis and automation. The microfluidic systems coupled with np-AgMSs as SERS substrates were applied for analytical applications to detect GSH and SCN^-. The developed system was found to be easy due to high specificity of Raman technique. A Raman spectrum provides a fingerprint that is unique to be specific for individual molecule. Therefore, sample preparation is not a requirement. Moreover, the results from analytical performance showed high accuracy and precision of the proposed method.

The synthesized np-AgMSs not only can be used as on-chip SERS substrates, but also can be possibly used as on-chip catalysts. Embedded np-AgMSs in a microfluidic channel could be used as electrochemical sensors for analyte preconcentration or direct detection of an analyte of interest. Moreover, static np-AgMSs could be applied for multi-step analysis because the particles are easily manipulated. Accordingly this research could be expanded into a board range of applications in future work.

REFERENCES

[1] A.J. Tüdos, G.A.J.B.a.R.B.M.S. Trends in Miniaturized Total Analysis Systems for Point-of-Care Testing in Clinical Chemistry. Lab on a Chip 1 (2001): 83–95.

[2] A. Khademhosseini, R.L., J. Borenstein, and J.P. Vacanti. Microscale Technologies for Tissue Engineering and Biology. PNAS 103(8) (2005): 2480–2487

[3] E.A. Jamil, P.K.S.a.K.F.J. Cells on Chips. Nature 442 (2006): 403-411.

[4] Greenway, L.M.a.G.M. Microfluidic Devices for Environmental Monitoring. Trends in Analytical Chemistry 24(9) (2005): 795-802.

[5] deMello, A.J. Control and Detection of Chemical Reactions in Microfluidic Systems. Nature 442 (2006): 394-402.

[6] D.R. Reyes, D.I., P.A. Auroux and A. Manz. Micro Total Analysis Systems. 1. Introduction, Theory, and Technology. Analytical Chemistry 74 (2002): 2623-2636.

[7] Mason, B.P., Price, K.E., Steinbacher, J.L., Bogdan, A.R., and McQuade, D.T. Greener Approaches to Organic Synthesis Using Microreactor Technology. Chemical Reviews 107(6) (2007): 2300-2318.

[8] Dendukuri, D., Pregibon, D.C., Collins, J., Hatton, T.A., and Doyle, P.S. Continuous-Flow Lithography for High-Throughput Microparticle Synthesis. Nat Mater 5(5) (2006): 365-369.

[9] Karnik, R., et al. Microfluidic Platform for Controlled Synthesis of Polymeric Nanoparticles. Nano Letters 8(9) (2008): 2906-2912.

[10] Tran, T.H., Nguyen, C.T., Kim, D.-P., Lee, Y.-k., and Huh, K.M. Microfluidic Approach for Highly Efficient Synthesis of Heparin-Based Bioconjugates for Drug Delivery. Lab on a Chip 12(3) (2012): 589-594.

[11] Xu, B.-B., et al. Localized Flexible Integration of High-Efficiency Surface Enhanced Raman Scattering (SERS) Monitors into Microfluidic Channels. Lab on a Chip 11(19) (2011): 3347-3351.

[12] Parisi, J., Su, L., and Lei, Y. In situ synthesis of silver nanoparticle decorated vertical nanowalls in a microfluidic device for ultrasensitive in-channel SERS sensing. Lab on a Chip 13 (2013): 1501–1508.

[13] Song, Y., Hormes, J., and Kumar, C.S.S.R. Microfluidic Synthesis of Nanomaterials. Microfluidics 4(6) (2008): 698-711.

[14] R. Gao, N.C., S.I. Chang, E.K. Leea and J. Choo. Real-Time Analysis of Diaquat Dibromide Monohydrate in Water with a SERS-Based Integrated Microdroplet Sensor. Nanoscale 6 (2014): 8781-8786.

[15] Schlucker, W.X.a.S. Medical Applications of Surface-Enhanced Raman Scattering. Physical Chemistry Chemical Physics 15 (2013): 5329-5344.

[16] Huh, Y.S., Chung, A.J., and Erickson, D. Surface Enhanced Raman Spectroscopy and Its Application to Molecular and Cellular Analysis. Microfluid Nanofluid 6 (2009): 285–297.

[17] Marre, S. and Jensen, K.F. Synthesis of Micro and Nanostructures in Microfluidic Systems. Chemical Society Reviews 39(3) (2010): 1183-1202.

[18] Bantz, K.C., et al. Recent Progress in SERS Biosensing. Physical Chemistry Chemical Physics 13(24) (2011): 11551–11567.

[19] Oh, Y.-J. and Jeong, K.-H. Optofluidic SERS Chip with Plasmonic Nanoprobes Self-Aligned Along Microfluidic Channels. Lab on a Chip 14(5) (2014): 865-868.

[20] Kleinman, S.L., Frontiera, R.R., Henry, A.-I., Dieringer, J.A., and Van Duyne, R.P. Creating, Characterizing, and Controlling Chemistry with SERS Hot Spots. Physical Chemistry Chemical Physics 15(1) (2013): 21-36.

[21] J. Parisi, Su, L., and Lei, Y. In-Situ Synthesis of Silver Nanoparticle Decorated Vertical Nanowalls in a Microfluidic Device for Ultrasensitive In-Channel SERS Sensing. Lab on a Chip 13 (2013): 1501–1508.

[22] Qing-ling Li, Li, B.-w., and Wang, Y.-q. Surface-Enhanced Raman Scattering Microfluidic Sensor. RSC Advances 3 (2013): 13015-13026.

[23] Tong, L., Righini, M., Gonzalez, M.U., Quidantbc, R., and Kall, M. Optical Aggregation of Metal Nanoparticles in a Microfluidic Channel for Surface-Enhanced Raman Scattering Analysis. Lab on a Chip 9 (2008): 193–195.

[24] G. Wang, C.L., L. Chen, H. Chon, J. Choo, J. Hong and A.J. deMello Surface-Enhanced Raman Scattering in Nanoliter Droplets: Towards High-Sensitivity Detection of Mercury (II) Ions. Analytical and Bioanalytical Chemistry 394(7) (2009): 1827-1832.

[25] L. Wu, Z.W., S. Zong and Y. Cui apid and reproducible analysis of thiocyanate in real human serum and saliva using a droplet SERS-microfluidic chip Biosensors and Bioelectronics 62 (2014): 13-18.

[26] G. Mettela, S.S., C. Narayanab and G.U. Kulkarni Nanocrystalline Ag Microflowers as a Versatile SERS Platform. Nanoscale (2014).

[27] K. Wongravee, et al. Nanoporous Silver Microstructure for Single Particle Surface-enhanced Raman Scattering Spectroscopy. RSC Adv 5 (2015): 1391–1397.

[28] Bourret, G.R., Goulet, P.J.G., and Lennox, R.B. Synthesis of Porous Metallic Monoliths Via Chemical Reduction of Au(I) and Ag(I) Nanostructured Sheets. Chemistry of Materials 23(22) (2011): 4954-4959.

[29] Lim, I.I.S., et al. Interparticle Interactions in Glutathione Mediated Assembly of Gold Nanoparticles. Langmuir 24(16) (2008): 8857-8863.

[30] G.G. Huang, M.K.H., X.X. Hanc and Y. Ozaki A Novel Reversed Reporting Agent Method for Surface-Enhanced Raman Scattering; Highly Sensitive Detection of Glutathione in Aqueous Solutions. Analyst 134 (2009): 2468–2474.

[31] Nie, S. and Emory, S.R. Probing Single Molecules and Single Nanoparticles by Surface-Enhanced Raman Scattering. Science 275(5303) (1997): 1102-1106.

[32] Dana Cialla, R.M.a.J.P. Application of Surface Enhanced Raman Spectroscopy for (bio)Analytical Devices.

[33] T. Vankeirsbilck, A.V., W. Baeyens, G. Van der Weken, F. Verpoort, G. Vergote, J.P. Remon. Applications of Raman Spectroscopy in Pharmaceutical Analysis. Trends in Analytical Chemistry 21(12) (2002): 869-877.

[34] Michaels, A.M., Nirmal, M., and Brus, L.E. Surface Enhanced Raman Spectroscopy of Individual Rhodamine 6G Molecules on Large Ag Nanocrystals. Journal of the American Chemical Society 121(43) (1999): 9932-9939.

[35] Chen, L. and Choo, J. Recent Advances in Surface-Enhanced Raman Scattering Detection Technology for Microfluidic Chips. Electrophoresis 29 (2008): 1815–1828.

[36] Zhang, J., Li, X., Sun, X., and Li, Y. Surface Enhanced Raman Scattering Effects of Silver Colloids with Different Shapes. The Journal of Physical Chemistry B 109(25) (2005): 12544-12548.

[37] Wang, Y. and Xia, Y. Bottom-Up and Top-Down Approaches to the Synthesis of Monodispersed Spherical Colloids of Low Melting-Point Metals. Nano Letters 4(10) (2004): 2047-2050.

[38] Radziuk, D. and Moehwald, H. Highly Effective Hot Spots for SERS Signatures of Live Fibroblasts. Nanoscale 6(11) (2014): 6115-6126.

[39] Li, Q.-l., Lib, B.-w., and Wangb, Y.-q. Surface-enhanced Raman scattering microfluidic sensor. RSC Advances 3 (2013): 13015–13026.

[40] Chung, T., Lee, S.-Y., Song, E.Y., Chun, H., and Lee, B. Plasmonic Nanostructures for Nano-Scale Bio-Sensing. Sensors 11(11) (2011): 10907.

[41] Radziuk, D. and Moehwald, H. Prospects for Plasmonic Hot Spots in Single Molecule SERS Towards the Chemical Imaging of Live Cells. Physical Chemistry Chemical Physics 17(33) (2015): 21072-21093.

[42] Yang, S. and Luo, X. Mesoporous Nano/micro Noble Metal Particles: Synthesis and Applications. Nanoscale 6(9) (2014): 4438-4457.

[43] Luo, X., et al. Volume Shrinkage Induced Formation of Porous Ag Sub-microcubes Via Solid-liquid Reaction for SERS. CrystEngComm 15(14) (2013): 2588-2591.

[44] Wongravee, K., et al. Nanoporous silver microstructure for single particle surface-enhanced Raman scattering spectroscopy†. RSC Adv 5 (2015): 1391–1397.

[45] Kneipp, K., Moskovits, M., and H.kneipp. Surface-Enhance Raman Scattering Physics and Applications. Vol. 103: Springer.

[46] Sharma, B., Frontiera, R.R., Henry, A.-I., Ringe, E., and Van Duyne, R.P. SERS: Materials, Applications, and the Future. Materials Today 15(1) (2012): 16-25.

[47] Gatemala, H., Thammacharoen, C., and Ekgasit, S. 3D AgCl Microstructures Selectively Fabricated Via Cl- Induced Precipitation from [Ag(NH3)2]+. CrystEngComm 16(29) (2014): 6688-6696.

[48] Gatemala, H., Thammacharoen, C., and Ekgasit, S. 3D AgCl microstructures selectively fabricated via Cl--induced precipitation from [Ag(NH3)2]+. CrystEngComm 16(29) (2014): 6688-6696.

[49] Lou, Z., et al. A 3D AgCl Hierarchical Superstructure Synthesized by a Wet Chemical Oxidation Method. Chemistry 18(50) (2012): 16090-6.

[50] You, H., Yang, S., Ding, B., and Yang, H. Synthesis of Colloidal Metal and Metal Alloy Nanoparticles for Electrochemical Energy Applications. Chemical Society Reviews 42(7) (2013): 2880-2904.

[51] Mettela, G., Siddhanta, S., Narayana, C., and Kulkarni, G.U. Nanocrystalline Ag Microflowers as a Versatile SERS Platform. Nanoscale 6(13) (2014): 7480-7488.

[52] Tao, A.R., Habas, S., and Yang, P. Shape Control of Colloidal Metal Nanocrystals. Small 4(3) (2008): 310-325.

[53] Liu, X., Xu, H., Xia, H., and Wang, D. Rapid Seeded Growth of Monodisperse, Quasi-Spherical, Citrate-Stabilized Gold Nanoparticles via H2O2 Reduction. Langmuir 28(38) (2012): 13720-13726.

[54] Alarcon, E., Griffith, M., and Udekwu, K.I. Silver Nanoparticle Applications, ed. Materials, E.: Springer, 2015.

[55] Gatemala, H., Thammacharoen, C., Ekgasit, S., and Pienpinijtham, P. 3D nanoporous Ag microstructures fabricated from AgCl microcrystal templates via concerted oxidative etching/re-deposition and galvanic replacement. CrystEngComm 18(35) (2016): 6664-6672.

[56] Whitesides, G.M. The Origins and The Future of Microfluidics. Nature 442 (2006): 368-373.

[57] Catarino, S., Lima, R., and Minas, G. 12 - Smart devices: Lab-on-a-Chip A2 - Rodrigues, Lígia. in Mota, M. (ed.)Bioinspired Materials for Medical Applications, pp. 331-369: Woodhead Publishing, 2017.

[58] Chen, L. and Choo, J. Recent advances in surface-enhanced Raman scattering detection technology for microfluidic chips. Electrophoresis 29 (2008): 1815–1828

[59] Lim, C., Hong, J., Chung, B.G., deMello, A.J., and Choo, J. Optofluidic Platforms Based on Surface-Enhanced Raman Scattering. Analyst 135(5) (2010): 809–1156.

[60] Leea, S., et al. Fast and Sensitive Trace Analysis of Malachite Green Using a Surface-Enhanced Raman Microfluidic Sensor. Analytica Chimica Acta 590(2) (2007): 139-144.

[61] Strehle, K.R., Cialla, D., Rösch, P., Henkel, T., Köhler, M., and Popp, J. A Reproducible Surface-Enhanced Raman Spectroscopy Approach. Online SERS Measurements in a Segmented Microfluidic System. Analytical Chemistry 79(4) (2007): 1542-1547.

[62] Weichun Ye, D.W., Hong Zhang, Feng Zhou, Weimin Liu. Electrochemical Growth of Flowerlike Gold Nanoparticles on Polydopamine Modified ITO Glass For SERS Application. Electrochimica Acta 55 (2010): 2004–2009.

[63] Chang, S., Combs, Z.A., Gupta, M.K., Davis, R., and Tsukruk, V.V. In situ Growth of Silver Nanoparticles in Porous Membranes for Surface-Enhanced Raman Scattering. ACS Applied Materials & Interfaces 2(11) (2010): 3333-3339.

[64] Galarreta, B., Tabatabaei, M., Guieu, V., Peyrin, E., and Lagugné-Labarthet, F. Microfluidic Channel with Embedded SERS 2D Platform for the Aptamer Detection of Ochratoxin A. Analytical and Bioanalytical Chemistry 405(5) (2013): 1613-1621.

[65] Lei Wu, Wang, Z., Shenfei Zong, and Cui, Y. Rapid and Reproducible Analysis of Thiocyanate in Real Human Serum and Saliva Using a Droplet SERS-Microfluidic Chip. Biosensors and Bioelectronics 62 (2014): 13-18.

[66] Q.L. Li, B.W.L.a.Y.Q.W. Surface-Enhanced Raman Scattering Microfluidic Sensor. RSC Advances 3 (2013): 13015-13026.

[67] Piorek, B.D., Lee, S.J., Santiago, J.G., Moskovits, M., Banerjee, S., and Meinhart, C.D. Free-Surface Microfluidic Control of Surface-Enhanced Raman Spectroscopy for the Optimized Detection of Airborne Molecules. Proceedings of the National Academy of Sciences 104(48) (2007): 18898-18901.

[68] K. Wongravee, H.G., C. Thammacharoen, S. Ekgasit, S. Vantasin, I. Tanabeb and Y. Ozaki. Nanoporous Silver Microstructure for Single Particle Surface-enhanced Raman Scattering Spectroscopy. RSC Advances 5 (2015): 1391–1397.

[69] Perrault, S.D. and Chan, W.C.W. Synthesis and Surface Modification of Highly Monodispersed, Spherical Gold Nanoparticles of 50–200 nm. Journal of the American Chemical Society 131(47) (2009): 17042-17043.

[70] Mei, X., Zheng, H., and Ouyang, J. Ultrafast Reduction of Graphene Oxide with Zn Powder in Neutral and Alkaline Solutions at Room Temperature Promoted by the Formation of Metal Complexes. Journal of Materials Chemistry 22(18) (2012): 9109-9116.

[71] David C. Duffy, J.C.M., Olivier J. A. Schueller, and George M. Whitesides. Rapid Prototyping of Microfluidic Systems in Poly(dimethylsiloxane). Anal Chem 70 (1998): 4974-4984.

[72] Pandey, P.C. and Singh, R. Controlled Synthesis of Pd and Pd-Au Nanoparticles: Effect of Organic Amine and Silanol Groups on Morphology and Polycrystallinity of Nanomaterials. RSC Advances 5(15) (2015): 10964-10973.

[73] Nau, R.N.D.U.P.W.M. Fluorescent Dyes and Their Supramolecular Host/Guest Complexes with Macrocycles in Aqueous Solution. Chemical Review 111 (2011): 7941–7980.

[74] Kulakovich, O.S., Shabunya-Klyachkovskaya, E.V., Matsukovich, A.S., Rasool, K., Mahmoud, K.A., and Gaponenko, S.V. Nanoplasmonic Raman Detection of Bromate in Water. Optics Express 24(2) (2016): A174-A179.

[75] Michaels, A.M., Jiang, and Brus, L. Ag Nanocrystal Junctions as the Site for Surface-Enhanced Raman Scattering of Single Rhodamine 6G Molecules. The Journal of Physical Chemistry B 104(50) (2000): 11965-11971.

[76] Iliescu, C., Mărculescu, C., Venkataraman, S., Languille, B., Yu, H., and Tresset, G. On-Chip Controlled Surfactant–DNA Coil–Globule Transition by Rapid Solvent Exchange Using Hydrodynamic Flow Focusing. Langmuir 30(44) (2014): 13125-13136.

[77] Nasanen, R. Equilibrium in Ammoniacal Solution of Silver Nitrate. Acta Chemica Scandinavica 1 (1947): 763-769.

[78] Wong, I. and Ho, C.-M. Surface Molecular Property Modifications for Poly(dimethylsiloxane) (PDMS) Based Microfluidic Devices. Microfluidics and Nanofluidics 7(3) (2009): 291.

[79] Xia, Y., Xiong, Y., Lim, B., and Skrabalak, S.E. Shape-controlled synthesis of metal nanocrystals: Simple chemistry meets complex physics? Angewandte Chemie International Edition 48(1) (2009): 60-103.

[80] Lou, Z., et al. One-Step Synthesis of AgCl Concave Cubes by Preferential Overgrowth Along ⟨111⟩ and ⟨110⟩ Directions. Vol. 48, 2012.

[81] Shevchenko, E.V., et al. Study of Nucleation and Growth in the Organometallic Synthesis of Magnetic Alloy Nanocrystals: The Role of Nucleation Rate in Size Control of CoPt3 Nanocrystals. Journal of the American Chemical Society 125(30) (2003): 9090-9101.

[82] Victor, K. and Mer, L. Nucleation in Phase Transitions. Industrial & Engineering Chemistry 44(6) (1952): 1270-1277.

[83] Borsook, H. and Ikeighley, G. Oxidation-Reduction Potential of Ascorbic Acid (Vitamin C). Physilogy: Borsook and Keighley 19 (1933): 875-878.

[84] Goia, D.V. Preparation and Formation Mechanisms of Uniform Metallic Particles in Homogeneous Solutions. Journal of Materials Chemistry 14(4) (2004): 451-458.

[85] Pakiari, A.H. and Jamshidi, Z. Nature and Strength of M−S Bonds (M = Au, Ag, and Cu) in Binary Alloy Gold Clusters. The Journal of Physical Chemistry A 114(34) (2010): 9212-9221.

[86] Kalburgi, C.V., Naik, K.L., Kokatnur, M.V., and Warad, S. Estimation and Correlation of Salivary Thiocyanate Levels in Healthy and Different Forms of Tobacco Users Having Chronic Periodontitis: A Cross-sectional Biochemical Study. Contemporary Clinical Dentistry 5(2) (2014): 182-186.

[87] Helrich, K. AOAC: Official Methods of Analysis of the Association of Official Analytical Chemists, ed. Boulevard, W. Vol. 1. United States of America, 1990.

APPENDIX

VITA

Miss Duangtip Lawanstiend was bond in 1989. She graduated a high school level from a Science division of Satri Si Suriyothai School, Bangkok, Thailand. She received a scholarship from King Mongkut's University of Technology Thonburi (KMUTT), Bangkok, Thailand to study bachelor's degree in Chemistry. After graduated from KMUTT, she received another scholarship from the Science Achievement Scholarship of Thailand (SAST) to continue her doctoral's degree in Chemistry at Chulalongkorn University, Bangkok, Thailand and finished in the year 2017.